Single-atom Iron-doped Graphene Quantum Dots Synthesized by a Green Chemical Method for High-efficiency Glucose Detection

Xinqi Li

A thesis

submitted in partial fulfillment of the

requirements for the degree of

Master of Science

Materials Science and Engineering

University of Washington
2023

Committee:
Miqin Zhang
Xiaojie Lin

Program Authorized to Offer Degree:

Department of Materials Science and Engineering

University of Washington

Abstract

Single-atom Iron-doped Graphene Quantum Dots Synthesized by a Green Chemical Method for High-efficiency Glucose Detection

Xinqi Li

Chair of the Supervisory Committee:
Miqin Zhang
Department of Materials Science and Engineering

Nanozymes have emerged as a promising class of nanomaterials that mimic the catalytic activity of natural enzymes. In this study, we present the synthesis and characterization of single Fe atom-doped graphene quantum dots (FeN/GQDs) as nanozymes for glucose detection. The FeN/GQDs are prepared through a facile hydrothermal method using pineapple leaves as a precursor, allowing for large-scale production. The synthesis process involves anchoring single Fe atoms to the graphene quantum dots through Fe-N coordinate bonds, which serve as catalytic sites. The catalytic activity of FeN/GQDs is evaluated by investigating their peroxidase-like (POD-like) activity using three chromogenic systems: TMB, OPD, and ABTS. The FeN/GQDs exhibit excellent catalytic efficiency, comparable to natural enzymes and other single atom nanozymes. The underlying catalytic mechanism is explored using the EPR-trapping technique. To demonstrate the practical application of FeN/GQDs, they are utilized as colorimetric nanomaterials for glucose detection. By combining glucose oxidase with FeN/GQDs, a colorimetric response is obtained and compared with other materials. The FeN/GQDs demonstrate high sensitivity and selectivity, making them suitable for glucose biosensing. The hydrothermal synthesis method employed in this study simplifies the production of FeN/GQDs, offering scalability and cost-effectiveness for large-scale

applications. Overall, this study introduces a novel synthesis method for FeN/GQDs as single atom nanozymes for glucose detection. The exceptional catalytic activity and stability of FeN/GQDs highlight their potential for various biomedical applications. The findings contribute to the development of nanozyme-based glucose detection technologies, enabling rapid and accurate glucose monitoring in clinical diagnostics and other related fields.

Acknowledgements

I would like to express our sincere gratitude to Professor Miqin Zhang for her guidance and support throughout this research. Her expertise in nanomaterials and valuable insights have been instrumental in shaping this study. Furthermore, I would like to express our sincere appreciation to the committee, Professor Miqin Zhang and Dr. Xiaojie Lin for their support and input throughout this research project. Their expertise and constructive criticism have been instrumental in shaping the direction and outcomes of this study. We are grateful for their time, expertise, and commitment to ensuring the rigor and excellence of our research.

I would also like to extend our appreciation to Dr. Guanyou Lin, PhD candidate Jianxi Huang, and Dr. Steve Chuang for their assistance and helpful discussions during this work, their input and support have been greatly appreciated. Furthermore, we would like to acknowledge the contributions of undergraduate researchers Mike Zhang, Tianxin Zhang, Tianyi Zhang, Octavia, and Carly. Their assistance in sample preparation, data collection, and literature review has been invaluable to the progress of this study.

Lastly, I would like to thank our families, friends, and colleagues for their continuous support and encouragement during this research endeavor. Their unwavering belief in our abilities has been a source of motivation throughout the process.

I acknowledge all the individuals who have contributed in various ways to this research but may not be mentioned explicitly. We are grateful for their support, whether intellectual, technical, or emotional.

This work would not have been possible without the collective efforts and collaboration of all those involved. We extend our heartfelt appreciation to everyone who has played a part in this research journey.

TABLE OF CONTENTS

Chapter 1. Introduction

Nanozymes are a novel class of nanomaterials that mimic the catalytic activity of natural enzymes[1-3]. While natural enzymes are essential biocatalysts that accelerate reactions in vivo and are crucial to metabolic processes, they often suffer from instability and inactivation under different temperature and pH conditions. Considering these limitations, researchers have turned to nanozymes as promising substitutes. One of the key advantages of nanozymes is their cost-effectiveness and ease of production. Unlike natural enzymes, which can be expensive and challenging to produce on a large scale, nanozymes can be synthesized in a more affordable and scalable manner. Furthermore, nanozymes exhibit enhanced stability compared to natural enzymes, making them suitable for a wide range of applications. Their stability enables them to maintain catalytic activity even under harsh conditions, such as high temperatures and extreme pH levels. These nanomaterials have gained significant attention due to their potential as alternatives to natural enzymes in various biomedical applications, including bioimaging[4-8], disease diagnosis and treatment[9-11], and biosensing[12-15]. They offer several advantages over natural enzymes, such as being inexpensive, easily produced, and highly stable.

Nanozymes were first discovered by Yan et al. in 2007, and since then, they have been extensively studied for their potential in biomedical applications. Among various types of nanozymes, single atom nanozymes have garnered significant attention for their high catalytic activity, stability, and unique molecular structure[14, 16, 17]. These nanozymes possess a unique molecular structure consisting of multiple active sites, which eliminates the need for extensive substrate-enzyme interactions and leads to highly efficient catalytic activity. Researchers have explored the use of different elements, including Au[9, 18], Pt[19, 20], Ag[21, 22], Co[23], and Mn[24], as catalytic centers in the synthesis of single atom nanozymes, and promising results have been obtained in various catalytic applications. Lin et al. synthesized core-shell structure nanoparticles loaded with monatomic gold via coordination bonds by self-assembly for combined chemotherapy and photodynamic therapy, which can releases

cisplatin and pyrolipid in a triggered manner to synergistically induce cancer cell apoptosis and necrosis[9]. Ming et al. developed a nanozyme-based bandage using single-atom Pt/CeO2 with a persistent catalytic activity for noninvasive treatment of neurotrauma, compared with CeO2 nanocluster, single atom doped NCs shows about 2-10 times catalytic ability[20]. In another study by Nie et al., a TiO2-supported single-atom nanozyme incorporating atomically dispersed Ag atoms (Ag-TiO2 SAN) was developed as a highly efficient antiviral nanomaterial. It demonstrated a remarkable adsorption capability of 99.65% towards SARS-CoV2 pseudovirus[21]. Additionally, Wang et al. designed cobalt/titanium oxide (Co/TiO2) single-atom nanozymes with cobalt atoms dispersed on nanoporous hollow TiO2 using a cation-exchange strategy. These nanozymes exhibited excellent biocompatibility and high tolerance towards biological media. The hollow structure of the nanozymes also facilitated the loading of drugs and imaging agents for image-guided chemo-chemodynamic therapy via intravenous injection[23]. Furthermore, Mn-based nanozymes[24] Mn/PSAE have been utilized for imaging and sensing applications, showing potential for early diagnosis and treatment of diseases.

However, despite the progress made with single atom nanozymes, some challenges still need to be addressed for their widespread use. One challenge is the reliance on noble metals, such as Au and Pt, as reaction sites, which can be costly and pose difficulties for large-scale production[25]. Additionally, concerns about the potential toxicity of noble-metal-based materials have been raised, as they may accumulate in living organisms and cause adverse effects[26]. To overcome these challenges, researchers are exploring non-noble metal-based nanozymes as alternatives, with a particular focus on Fe-based nanozymes. The use of Fe-based materials offers a more sustainable and environmentally friendly approach, and further investigation is needed to fully exploit their catalytic potential in biomedical applications.

Fe is a readily available and low-cost element, making it a promising alternative to Au, Pt, and Cu for various catalytic systems[26, 27]. Its abundance in the Earth's crust and economical price makes Fe-based nanozymes

attractive for large-scale production and application. Moreover, Fe-based nanozymes have demonstrated high stability and catalytic activity in aqueous solutions, rendering them suitable for biomedical usage in real biological systems[28-30].The synthesis of Fe-based single atom nanozymes has emerged as a rapidly developing field, with a growing body of research indicating their potential for a wide range of applications. Li et al. utilized a high-temperature gas-migration strategy to create porphyrin-like single iron (Fe) sites on N-doped carbon nanomaterials. This innovative approach resulted in the formation of nanomaterials with exceptional peroxidase, oxidase, catalase enzyme-like, and Fenton-like activities[31]. In another study, Wu et al. successfully obtained single Fe atom nanozymes by utilizing Fe(phen)x as precursors with a support-sacrificed strategy, followed by pyrolysis and pickling at 600℃[32]. However, it is important to note that the synthesis of Fe-based single atom nanozymes typically requires high-temperature and high-pressure conditions[31-34], which can be challenging and not suitable for large-scale production[26]. Therefore, the development of a simple and scalable synthesis method for Fe-based single atom nanozymes is necessary to fully realize their potential for large-scale applications. This would enable researchers and industry professionals to harness the advantages of Fe-based nanozymes in a cost-effective and efficient manner.

In this study, the work is mainly divided into the following two parts:

First, we will introduce a novel synthesis method for preparing single Fe atom-doped graphene quantum dots (FeN/GQDs) that allows for large-scale production. The aim of this part is to investigate whether there is Metal-Nitrogen single atom structure successfully doped on the as-synthesized FeN/GQDs nanozymes obtained by hydrothermal method and quantify the catalytic activity of FeN/GQDs. Variety of detection methods will be employed to characterize the physicochemical properties of FeN/GQDs and further obtain its single atom structure. To understand their catalytic properties, we employed three main chromogenic systems, namely TMB, OPD, and ABTS, to monitor the peroxidase-like catalytic activity of FeN/GQDs. Furthermore, EPR-trapping technique were

employed to gain insights into the underlying mechanism.

Second, to evaluate the performance of FeN/GQDs in practical applications, we utilized them as colorimetric nanozymes for biosensing, with glucose detection serving as the detection model. Glucose plays a crucial role in the body's metabolic processes, and maintaining proper glucose levels is essential for good health[35]. Various methods have been explored for glucose detection, including colorimetry[36], fluorescence[37], surface-enhanced Raman scattering[38], chemiluminescence[39], and electrochemistry[40]. Colorimetric techniques utilizing nanozymes offer several advantages, such as visual visibility, convenience, and low cost, making them an attractive option for biosensing glucose[41]. In this study, FeN/GQDs will combine with glucose oxidase as a potential colorimetric glucose detection system.

The successful production of FeN/GQDs nanozymes by hydrothermal method brings more opportunities to further understand the underlying mechanism and utilize the single atom nanozymes. By replacing traditional high-temperature pyrolysis methods with a cost-effective hydrothermal synthesis, researchers have established a bridge for further understanding and designing single-atom nanozymes. This breakthrough synthesis approach not only enables the exploration of the catalytic potential of FeN/GQDs but also facilitates the development of innovative strategies for precise treatments and sensitive diagnostic platforms. The exceptional catalytic properties and unique structure of FeN/GQDs hold great promise in advancing biomedical applications, offering opportunities for targeted therapies and accurate disease detection.

Chapter 2. Glucose detection and nanozymes

1. Glucose detection

Glucose plays a crucial role in the physiological and pathological processes of the human body, as an indispensable energy source[42]. In clinical diagnostics[43], Complications caused by abnormal blood glucose

concentration have attracted much attention. If the blood sugar content is too high, it will cause diabetes, heart disease, kidney disease and nerve damage and other diseases. If the blood sugar level is too low, it can also lead to stroke or other vascular diseases that seriously harm the health of the body. Among them, diabetes is a great threat to human health, and how to solve diabetes is a worldwide problem. Therefore, the study of glucose sensor with high sensitivity, strong selectivity and good stability has important academic significance and broad application prospects.

1.1 Traditional detection methods

The principle of traditional glucose detection technology can be broadly categorized into two methods: photochemical (colorimetry) and electrochemical. Both methods require enzymatic catalysis and the acquisition of a blood sample. The main distinction lies in the form of the signal. In the photochemical method, the glucose concentration is determined by measuring the strength of the light signal caused by the current changes resulting from the oxidation of reduced chromogen to oxidized chromogen. On the other hand, the electrochemical method relies on measuring the strength of the electronic signal caused by the current changes resulting from the production and transfer of electrons during the catalytic decomposition of glucose.

In the photochemical method, glucose oxidase (GOD) and peroxygenase enzymes are immobilized on the test paper of the blood glucose meter. Under the action of glucose oxidase, glucose is broken down to produce hydrogen peroxide (H2O2). The oxidase catalyzes the oxidation of the reduced chromogen, resulting in a change in absorbance. The glucose concentration is then calculated based on the absorbance change.

In the electrochemical method, the test paper's electrode surface is coated with glucose oxidase (GOD) and glucose dehydrogenase (GDH). When blood enters the reaction zone through the blood sample, glucose

undergoes catalytic decomposition by GOD and GDH, leading to the generation of electrons. These electrons are transferred to the electrode through the dielectric, causing a change in the current flowing through the electrode. The current value is linearly correlated with the blood glucose concentration, enabling the calculation of glucose levels.

1.2 Optical detection methods

The optical method offers several advantages, including non-invasiveness, non-pollution, low cost per single detection, rapid detection speed, and no requirement for reagents and consumables. It holds great promise as a quantitative detection method. Optical detection methods typically utilize light of specific wavelengths as carriers of information. When this light interacts with human tissue in the target region, it generates signals that bear biochemical information related to the tissue. These signals are received by high-performance sensors, and mathematical analysis is employed to establish a stable correlation between human biochemical information and optical signals. By studying this correlation, we can utilize the signals to predict the quantity of the corresponding component in the human body. Currently, there are various optical methods employed for glucose detection, such as Raman spectroscopy, polarizing optical rotation, photoacoustic spectroscopy, photothermal effect, optical coherence tomography, and infrared absorption spectroscopy. These methods offer diverse approaches to capturing optical signals and extracting glucose-related information. Each method has its strengths and limitations, and ongoing research aims to optimize their performance and explore their applicability in glucose detection.

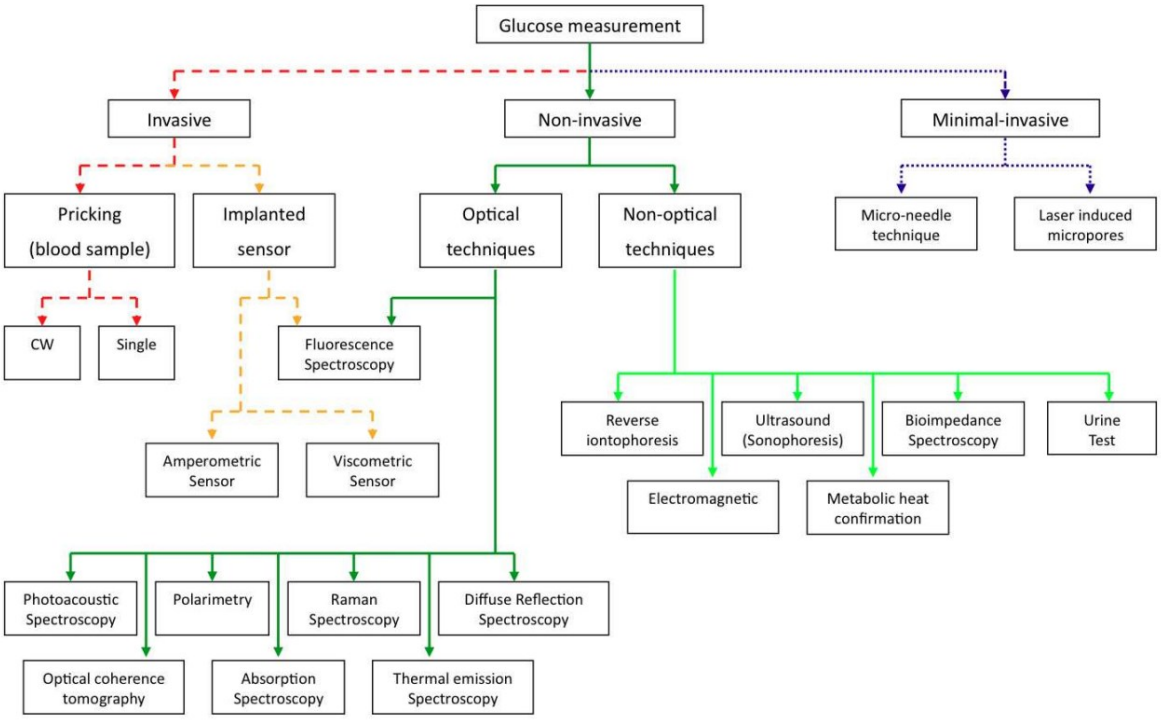

Scheme 1. Overview of possible techniques and active research areas for glucose measurements Reprinted from Ref. Peng et al.[44]

2. Nanozymes

As a very important biocatalyst, enzymes exist in all aspects of nature and human life and participate in various life phenomena in living objects. Due to the high specificity and catalytic efficiency of enzymes on substrates under optimal conditions, they have been widely used in disease diagnosis, clinical medicine and industrial production and life. However, most natural enzymes are composed of proteins, so they are extremely unstable in the harsh external environment and are easily denatured to lose enzyme activity. In addition, the separation and extraction process of natural enzymes is still complex and high cost, and the final production of natural enzymes is not easy to preserve, which restricts the practical application of natural enzymes. So more and more researchers are turning their attention to artificially producing substances that can mimic the action of natural enzymes. In 1970, Ronald Breslow first proposed the concept of artificial simulated enzymes, which is a very important time point in bionic chemistry, aiming to simulate the basic properties of natural enzymes with

artificially prepared and efficient alternative materials. In the past few decades, various artificial enzymes have been prepared to act in place of natural enzymes.

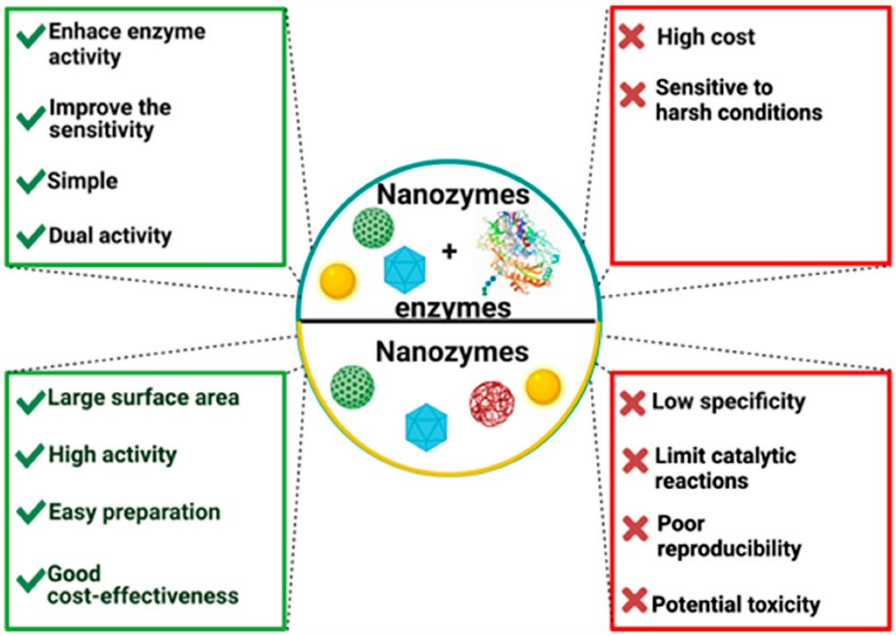

Scheme 2. Advantages and disadvantages of nanozymes and Enzymes pool. Reprinted from Ref. Alvarado-Ramírez et al.[45]

2.1 Classification of nanozymes

Since Gao et al.[46] first proposed in 2007 that magnetic ferric oxide nanoparticles (Fe3O4 NPs) have intrinsic POD-like properties, nanozymes have become a research hotspot. The current nanomaterial peroxidase mimics can be roughly divided into the following categories.

2.1.1 Metallic oxide/sulfide-based

Metallic oxide/sulfide-based nanozymes refer to a class of nanozymes composed of metal elements combined with oxide or sulfide structures. In 2007, Gao et al. [46] first found that Fe_3O_4 NPs actually exhibited an inherent peroxisase-like activity. Shortly after Gao et al. 's report was published, Wei and Wang[47] developed a new sensing platform, using Fe_3O_4 NPs as a peroxisase simulator. For H2O2 and glucose detection. Ahme et al. [48] showed a green route, which can be synthesized by simple hydrothermal treatment of Fe3O4 quantum dots. The fluorescence emission spectrum, UVV spectrum and circular

dichroism spectrum of Fe3O4 quantum dots are located at 419, 395 and 335 nm, respectively. X-ray photoelectron spectroscopy shows that when Fe3O4 NPs is converted to Fe3O4 quantum dots, the ratio of Fe (II) to Fe (III) increases. Fe3O4 quantum dots have very high peroxidase activity and the sensitive detection limit for H2O2 is 3.87 nM. Kinetic studies show that Fe3O4 quantum dots have higher affinity for TMB than standard HRP.

2.1.2 Noble metal-based

Some precious metal nanomaterials have metal catalytic active sites and also exhibit enzyme-like activities. Jv et al. [49] first found that Au NPs possessed POD-like simulated enzyme activity, and applied it to glucose detection, opening the door of precious metals as nanozymes. Mvango et al.[50] successfully synthesized CuO-Au nanoalloys and characterized them, confirming the formation of an alloy of gold and copper, in which copper exists in the form of copper oxide. By studying the properties of the synthesized nanoalloy, it was determined that it had pod-like activity. The detection limit of glucose was 6.75μM through the sensing platform constructed by CuO-Au nanoalloy.

2.1.4 Carbon-based

Compared with the previous two nanomaterials, carbon-based nanomaterials have many kinds, and have the advantages of high stability, low cost, good biocompatibility, and easy synthesis and modification.

2.1.5 Single atom nanozymes

Single-atom nanozymes have the largest atomic utilization efficiency, unique geometric structure and fully exposed active sites, making them increasingly research hotspot.

2.2 Nanozymes with glucose detection

In recent years, the emergence of nanozymes as alternatives to natural enzymes has revolutionized glucose detection. Various types of nanozymes have been explored for glucose detection, including metal-based nanozymes, carbon-based nanozymes, and hybrid nanozymes. Metal-based nanozymes, such as gold nanoparticles (AuNPs) [51], silver nanoparticles (AgNPs)[52], and copper nanoparticles (CuNPs), possess

excellent catalytic activity and can be easily modified to enhance their glucose sensing capabilities. Carbon-based nanozymes[53], such as graphene oxide (GO) and carbon nanotubes (CNTs), offer high surface area, electrical conductivity, and biocompatibility, enabling sensitive and selective glucose detection. Hybrid nanozymes, composed of a combination of different nanomaterials, combine the advantages of each component, resulting in enhanced catalytic performance and improved glucose sensing.

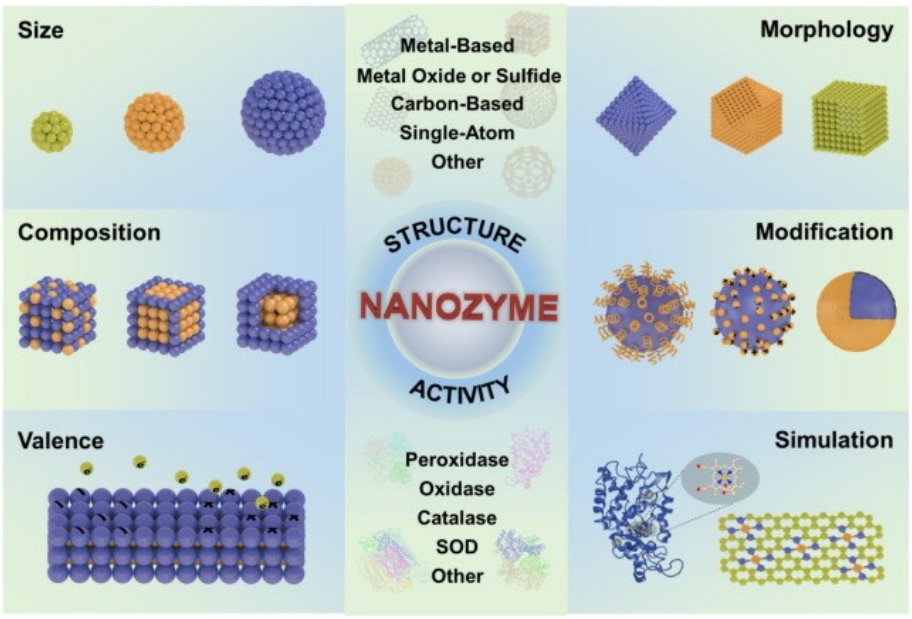

Scheme 1. Schematic illustration shows the category of nanozymes and the structure-activity relationship of nanozymes. Reprinted from Ref. Wang et al.[54]

The detection principles of nanozymes-based glucose assays vary depending on the nanomaterial used and the sensing mechanism employed[55]. For example, some nanozymes utilize the oxidation of glucose to generate reactive oxygen species (ROS), which can be detected electrochemically or calorimetrically. Others employ the reduction of a suitable substrate, leading to a change in electrical or optical signals. Additionally, some nanozymes function through a combination of enzymatic-like activity and specific recognition elements, such as aptamers or antibodies, enabling highly selective and sensitive glucose detection.

The development of novel nanozyme-based glucose detection platforms has opened up new possibilities for rapid, sensitive, and selective glucose monitoring. These platforms offer several advantages, including simple sample preparation, high stability, low cost, and compatibility with portable and miniaturized devices.

Furthermore, nanozyme-based glucose detection holds great potential for integration with emerging technologies, such as wearable devices, point-of-care testing devices, and lab-on-a-chip systems, enabling real-time monitoring and personalized healthcare applications.

Glucose detection is a critical aspect of various fields, and the advent of nanozymes has revolutionized the field by offering improved stability, sensitivity, and versatility compared to traditional enzyme-based assays. Nanozyme-based glucose detection platforms hold tremendous promise for the development of advanced sensing technologies, enabling rapid and accurate glucose monitoring in clinical, food, and biotechnological applications. The utilization of metal-based, carbon-based, and hybrid nanozymes has expanded the range of possibilities for glucose detection, allowing for enhanced catalytic activity and improved sensing capabilities. These nanozyme-based glucose assays operate through various detection principles, including the generation of reactive oxygen species, signal changes in electrical or optical properties, and the integration of recognition elements for selective detection.

In summary, nanozyme-based glucose detection represents a promising and transformative approach in the field of glucose monitoring. By harnessing the catalytic activity and inherent advantages of nanozymes, researchers and industry professionals are advancing the development of highly efficient, reliable, and cost-effective glucose sensing platforms with significant implications for various applications.

Chapter 3. Motivation

Fe-N_x (Iron with Nitrogen coordination) nanozymes represent a unique class of single atom nanozymes with remarkable catalytic properties. However, existing single atom nanozymes, particularly those based on noble metals, have certain limitations, such as high cost and the requirement of high-temperature synthesis methods (>800-1000°C) with nitrogen protection, which hinder their large-scale production. (**Table 1**) In light of these challenges, the motivation behind this study is threefold:

1). Innovative Material Design: The development of FeN/GQDs as a novel material represents a significant breakthrough. These single atom nanozymes offer promising catalytic capabilities, but they also have inherent flaws. By addressing the drawbacks of conventional single atom nanozymes, such as the high cost and challenging synthesis conditions, FeN/GQDs provide a unique opportunity to advance the field of single atom nanozyme research.

2). Simplified Synthesis Approach: The aim of this study is to establish a simplified synthesis method for FeN/GQDs, which can overcome the limitations associated with existing approaches. By developing a facile and scalable synthesis route, it opens up new possibilities for large-scale production of single atom nanozymes. This innovative synthesis pathway not only contributes to the field of nanozyme research but also provides a new perspective for the synthesis of other single atom nanozymes.

3). Application in Biosensing and Glucose Detection: The integration of FeN/GQDs into biosensing, specifically glucose detection, is another driving force behind this study. Glucose detection plays a crucial role in various fields, including clinical diagnostics and food industry applications. By utilizing FeN/GQDs as a colorimetric nanomaterial in glucose detection, it offers several advantages, such as visual visibility, convenience, and cost-effectiveness. The development of this nanomaterial platform for glucose detection provides a practical application and showcases the potential of FeN/GQDs in advancing biosensing technologies.

By addressing the challenges associated with conventional single atom nanozymes and leveraging the advantages of FeN/GQDs, this study aims to contribute to the field of nanozyme research, provide new insights into the synthesis of single atom nanozymes, and explore their potential in biosensing applications, particularly glucose detection.

Table 1. Comparison of the synthesis process of different Single Iron atom nanozymes.

Single Fe Nanozymes	Synthesis Condition	Precursors	Application

Fe-N-C Sazymes[56]	Pyrolysis, 900°C, N2 atmosphere	Glucose, DICY, and FeCl2·4H2O	H2O2 detection
FeBNC SACs[15]	Pyrolysis	glucose, dicyandiamide (DICY), boric acid, iron dichloride	detection of acetylcholinesterase
Fe-SANs[28]	Pyrolysis, 700°C, N2 atmosphere	1,10-phenanthroline monohydrate (O-Phen), zinc acetate dihydrate (Zn(OAc)2·2H2O), phthalocyanine (FePc)	drug detection
CNT/FeNC[57]	Pyrolysis	CNTs, Pyrrole, Fe(NO3)3, NaCl	Biosensing
Fe-Zn ZIFs/Fe-N/C[34]	ZIFs Pyrolysis	Fe(NO3)3·9H2O, Zn(NO3)2·6H2O, MIM	detection of alkaline phosphatase
Fe–N–C SANs[58]	Pyrolysis, 900°C, N2 atmosphere	ferric chloride, polyvinylpyrrolidone, potassium chloride, or sodium chloride	selective determination of antioxidants
Fe-N-C Sazyme[59]	calcination, 350°C + Pyrolysis,800°C	Pluronic F127, dopamine hydrochloride, (NH4)2Fe(SO4)2·6H2O, 1,3,5-trimethylbenzene, NH3·H2O	antibacterial therapy
Porphyrin-Like FeSAzyme[60]	pyrolysis, 800 °C	Fe(acac)3-ZIF-8@mSiO2	tumor therapy
Fe-N-C SAN[61]	Pyrolysis, 900°C, N2 atmosphere	Zn(NO3)2·6H2O, Fe(NO3)3·6H2O, methylimidazole	Biosensing
SA-Fe/NG[62]	pyrolysis, 800 °C	Urea, ferrous acetate, 1,10-phenanthroline monohydrate	detection of Cr(VI)
Fe-N/C Sazyme[63]	Pyrolysis, 900°C, N2 atmosphere	Fe(acac)3@ZIF-8	Detection of malathion
Fe-N/S-C[30]	400°C carbonized peanut shells, pyrolysis, 800 °C	peanut shells, Fe(NO3)2.9H2O,CO(NH2)2	Colorimetric detection of GSH and Hg2+
FeSA-HNCS[64]	Pyrolysis, 900°C, N2 atmosphere	SiO2 nanospheres, TEOS, DA, Fe(acac)3	cell therapy
FeCu-DA/NC[65]	Pyrolysis	metal salts (Fe, Cu), PVP and nano-CaCO3	oxygen reduction

FeN/GQDs[a]	Hydrothermal, 190℃	Plant leaves, $FeCl_2$	Biosensing

[a]: This work

Chapter 4. Rational Design of FeN/GQDs nanozymes

The synthesis process involves a facile hydrothermal method using pineapple leaves as a precursor. As the main components of pineapple leaves, glucose and polyphenols has been proved with ability of chelating metal ions, which can help forming the intermedia precursors[66, 67]. To extract the glucose and polyphenols, DMF was chosen since it cannot only help extraction, but also can prevent the over oxidation of Fe ions[68]. Through tip sonicating treatment, the intermedia precursors of Fe^{2+} ions with glucose/polyphenols are formed. Then treat with 9 hr 180℃ hydrothermal synthesis, we can have Fe/N structure anchoring on the GQDs frame. The graphene quantum dot support provides mechanical stability, while the nitrogen coordination structure protects the Fe atoms from oxidation and degradation.

Chapter 5. Materials and Methods

1. Chemical Reagents

All the chemical reagents used in this study were of analytically pure grade and were used without further purification. The following reagents were used: N,N-Dimethylformamide (DMF, Sigma-Aldrich), Iron(II) chloride (FeCl2, Sigma-Aldrich), hydrogen peroxide (H2O2, 30% concentration, Sinopharm), ethanol, TMB (3,30,5,50-tetramethylbenzidine, 99% purity, Macklin), ABTS (2,20-azinobis-3-ethylbenzthiazoline-6-sulphonate, 98% purity, Sigma-Aldrich), OPD (o-phenylenediamine, 98% purity, Sigma-Aldrich), ethanol (99.70% purity, Sinopharm), acetic acid (HAc, 99.5% purity, Sigma-Aldrich), sodium acetate (NaAc, Sigma-Aldrich), glucose (99.0% purity, Sigma-Aldrich), PBS buffer (1X, Fisher Scientific), dimethyl sulfoxide (DMSO, HPLC grade,

Fisher Scientific), glucose oxidase (GOx, Sigma-Aldrich), and horseradish peroxidase (Sigma-Aldrich). The pineapple leaves (Ananas comosus) used in this study were sourced from pineapples purchased from Costco.

2. Preparation of nanozymes

FeN/GQDs were synthesized using an environmentally friendly hydrothermal method. Ananas comosus leaves were chosen as a sustainable source of carbon and nitrogen and were thoroughly washed and finely chopped prior to utilization. Dimethylformamide (DMF) was employed as the solvent, serving multiple purposes including nitrogen supplementation, reduction, and metal protection33.To initiate the synthesis of FeN/GQDs, 2 grams of the chopped leaves were subjected to ultrasonication in a 20-milliliter DMF solution, resulting in an extract solution. Subsequently, the extract solution was combined with 1 gram of FeCl2 and subjected to further sonication to ensure a homogeneous mixture. This well-mixed solution was then transferred into a 50-milliliter PTFE liner, where it underwent a hydrothermal reaction at a temperature of 190°C for a duration of 8 hours. The final product was obtained through a purification process that involved multiple rounds of centrifugation and dialysis to eliminate small molecules and bulk particles. The resulting solution, containing nanoparticles with sizes ranging from 10 to 15 nanometers, was freeze-dried to yield the final powdered FeN/GQDs sample for subsequent experimental investigations.

3. Characterization and Measurement

To comprehensively characterize the FeN/GQDs, a series of analytical techniques were employed to determine their size, structure, morphology, composition, and optical properties.

Dynamic light scattering (DLS) analysis was performed using a Zetasizer Nano-ZS instrument (Malvern Instruments, Worcestershire, UK) in NaAc-Hac buffer. This technique allowed for the determination of the average particle size and zeta potential of the FeN/GQDs. Additionally, the Polydispersity Index (PDI) was collected as an indicator of the uniformity degree of the nanoparticles.

Transmission electron microscopy (TEM) using a Ted Pella instrument (Redding, CA, USA) was utilized to observe the morphological features of the FeN/GQDs. High-resolution TEM (HR-TEM) images were acquired to provide a detailed view of the FeN/GQDs. Furthermore, element mapping was conducted to confirm the presence and spatial distribution of Fe, N, and C in the samples.

Ultraviolet-visible spectroscopy (UV-VIS) was carried out using an 8453 Diode Array UV-Vis Spectrophotometer (Agilent) to determine the optical properties of the FeN/GQDs. The absorption spectra of the FeN/GQDs in NaAc-Hac buffer were recorded to analyze their optical characteristics. Additionally, colorimetric methods were employed to evaluate the POD-like properties of the FeN/GQDs.

Photoluminescence spectroscopy (PL) was performed using an LS-55 Luminescence Spectrophotometer (Perkin Elmer) to study the photoluminescence properties of the FeN/GQDs. The PL spectra were recorded to determine their emission characteristics, assess their potential as glucose detection nanozymes, and understand their luminescent behavior.

Fourier-transform infrared spectroscopy (FTIR) analysis was conducted using a Nicolet 6700 spectrometer (Thermo Scientific Inc., Waltham, MA, USA) to investigate the functional groups present in the FeN/GQDs. The FTIR spectra were recorded with a resolution of 4 cm^−1, averaging the signal over 64 scans. The FeN/GQDs samples were prepared as pellets with KBr for analysis, enabling the identification of specific functional groups and the analysis of their chemical structure.

Raman spectroscopy was performed using an inVia™ confocal Raman microscope (RENISHAW) with a 514 nm laser excitation source to study the vibrational properties of the FeN/GQDs. The Raman spectra were recorded to determine their vibrational characteristics, providing valuable insights into their structural features and chemical bonding.

X-ray photoelectron spectroscopy (XPS) was performed using an AXIS Ultra DLD / Surface Science Instruments

S-Probe instrument (Kratos) to study the composition and electronic structure of the FeN/GQDs. This technique provided valuable information about the chemical composition, oxidation states of the elements present, and the electronic environment of the FeN/GQDs.

X-ray absorption near-edge structure (XANES) analysis was employed to obtain detailed information on the valence and coordination of the FeN/GQDs. The X-ray absorption fine structure spectra (Fe K-edge) were collected at the 7-BM beamline.

4. Peroxidase-like Activity Evaluation and Kinetic Analysis of Nanozymes and HRP

The peroxidase (POD)-like activity of FeN/GQDs and NGQDs was evaluated using a standard assay. In this typical POD-like activity assay, the nanozymes (FeN/GQDs and NGQDs) were added to a solution containing TMB as the substrate and H2O2 in a buffer solution (0.1 M HAc-NaAc, pH 3.6). The absorbance of the blue-colored product at 652 nm was measured using a UV-vis spectrophotometer at specific reaction times. To initiate the chromogenic reactions, a specific amount of FeN/GQDs and NGQDs was mixed with a 1 mL buffer solution containing 10 μL of TMB (0.4 mM) and H2O2 (100 μM). The standard steady-state kinetic tests were carried out at 37 °C in a 1 mL reaction buffer solution. Subsequently, a 10 μL solution of GQDs-based nanozymes (1 mg/mL) was added to initiate the reaction with TMB and H2O2 substrates. Similarly, the reaction kinetics of FeN/GQDs and NGQDs were evaluated by adding 10 μL aliquots of H2O2 (10 mM, prepared from a 30% v/v stock solution) and varying volumes (0.5, 1, 2, 5, 7, 8, 10, 12.5, 15, 20, 50 μL) of TMB solution (in ethanol, 10 mg/mL). The reaction kinetics of FeN/GQDs and NGQDs were assessed by adding 10 μL aliquots of H2O2 (10 mM, prepared from a 30% v/v stock solution) and varying concentrations of H2O2 (0.5, 1, 2, 5, 10, 20, 30, 40, 50, 60, 70, 80, 100, 150, 200, 500 μL) while keeping the TMB (10 μL of 10 mg/mL) and GQDs-based catalyst (10 μL of 1 mg/mL) conditions constant. The POD-like kinetic assays were performed under these conditions, and the absorbance of each reaction was measured at various time points during the process. The characteristic Michaelis–Menten

constant (Km) and velocity (Vmax) were calculated by Lineweaver-Burk plot (Equation. 1) using the saturation curve in Origin Pro 2021b.

$$1/v=Km/Vmax*1/[S] +1/Vmax \qquad \text{(Equation 1)}$$

Where, v is the initial reaction velocity, Vmax is the maximum reaction velocity, and [S] is the substrate concentration. The physical meaning of Km value is the substrate concentration when the reaction speed reaches half Vmax. The POD-like activity of FeN/GQDs and NGQDs was investigated in buffer solutions with pH values ranging from 2 to 12, using the same substrate conditions. Additionally, the temperature dependence effect on the POD-like activity was assessed over a temperature range of 17 °C to 60 °C. For ABTS and OPD assay protocol, see details in supplementary information.

As a control experiment, horseradish peroxidase (HRP) as natural enzymes were tested using the same process above to compare with the FeN/GQDs nanozymes in this assay.

5. Free Radical Identification

To investigate the generation of free radicals during the catalytic activity of FeN/GQDs, Electron Spin Resonance (EPR) analyses were performed using a Bruker EPR instrument at room temperature. In the EPR experiments, a mixture of 5,5-dimethyl-1-pyrroline N-oxide (DMPO) and FeN/GQDs was prepared in a pH 3.6 buffer solution. The mixture was incubated at 30°C for 5 minutes to allow for proper interaction. The reaction was then initiated by adding a 10 mM H2O2 solution and further incubated for 5 minutes before transferring it to a capillary tube for EPR analysis. The final concentrations of each component in the reaction mixture were 100 mM DMPO, 20 μg FeN/GQDs, and 1 mM H2O2. During the EPR analysis, the instrument was set to the following parameters: 1 G field modulation, a scan range of 200 G, and a microwave power of 20 mW for the detection of spin adducts using spin traps. The spin-trap DMPO was employed to verify the formation of hydroxyl radicals (OH•) during the degradation of H2O2 in the presence of FeN/GQDs, NGQDs, and HRP in a 1.0 ml NaAc-HAc buffer (0.1 M,

pH 3.6).

6. Colorimetric Detection of Glucose

A colorimetric glucose detection system was developed for potential biosensing applications, utilizing the synergistic action of glucose oxidase (GOx), FeN/GQDs, and 3,3',5,5'-tetramethylbenzidine (TMB). The detection process is based on the enzymatic oxidation of glucose by GOx, resulting in the production of glucose-acid and hydrogen peroxide (H2O2) as a byproduct. FeN/GQDs act as catalysts, enhancing the conversion of H2O2 into highly reactive hydroxyl radicals. These hydroxyl radicals then react with TMB, leading to a distinct color change from colorless to blue (Scheme 1). The colorimetric glucose detection procedure involved the following steps:

1). A mixture containing 10 μL of GOx (10 mg/mL) and 100 μL of glucose buffer solutions at varying concentrations was incubated at 37 °C for 30 minutes.

2). To the glucose mixture solution, 10 μL of TMB (30 mM), 10 μL of FeN/GQDs dispersion (1 mg/mL), and 0.79 mL of 0.1 M HAc-NaAc buffer (pH 3.7) were added.

3). The reaction solution was further incubated at 37 °C for 6 minutes, followed by the measurement of absorbance values using a UV-vis spectrophotometer. The color changes corresponding to different glucose concentrations (ranging from 1 to 1000 μM) were monitored by analyzing the absorption spectra, specifically focusing on the intensity at 652 nm. Visual observation of the color change was also performed, allowing for glucose detection without the need for specialized equipment.

4). To ensure accuracy and reliability, the measurements were repeated three times for each glucose concentration tested. The resulting absorbance values and corresponding color changes were analyzed and used to establish a calibration curve for glucose quantification.

In addition to the commonly used substrate TMB, the colorimetric glucose detection system also employs o-phenylenediamine (OPD) and 2,2'-azino-bis(3-ethylbenzothiazoline-6-sulfonic acid) (ABTS) as alternative

substrates. The OPD and ABTS assay use the same protocol as TMB with different substrate concentrations.

7. Stability and reusability test

Experiments were designed to investigate the stability and reusability of FeN/GQDs nanozymes. Colloidal stability was measured with DLS. For catalytic activity, the FeN/GQDs was store under room temperature for 30 days, under optimal conditions for TMB assay, UV-Vis absorbance at 560 nm was recorded periodically. For reusability experiments, the recycled FeN/GQDs was collected via centrifugation, washing, and drying after TMB assay.

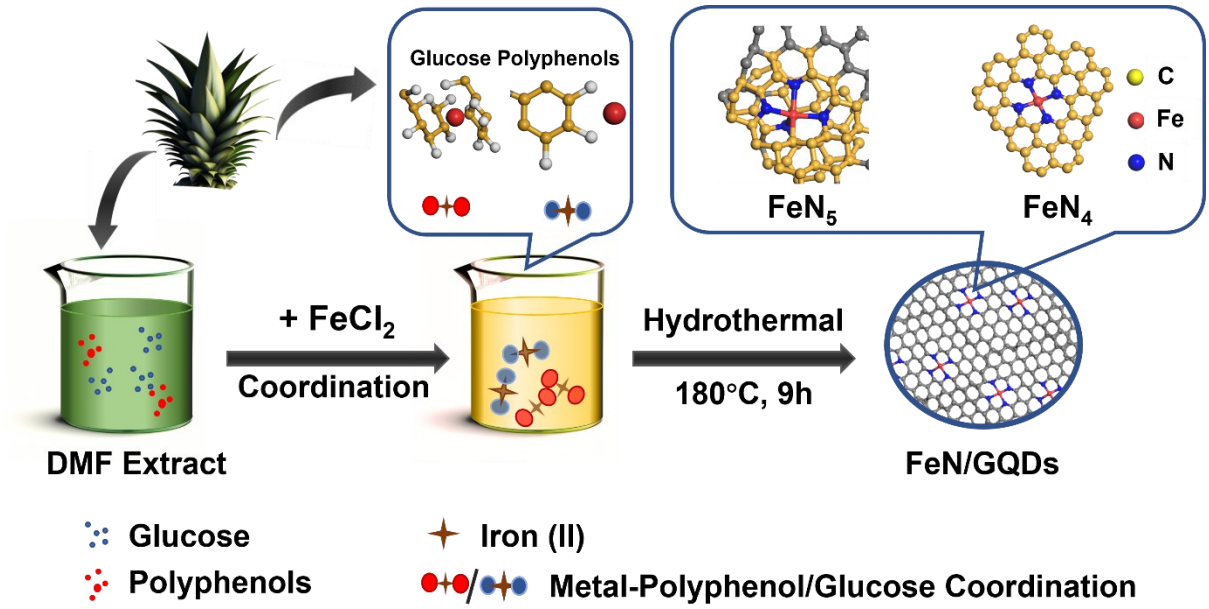

Scheme 5. Illustration of the preparation process of FeN/GQDs nanozymes.

Chapter 6. Results and Discussion

1. Characterization of FeN/GQDs nanozymes

The synthesis of Fe-N doped graphene quantum dots (FeN/GQDs) involves a hydrothermal process utilizing Ananas comosus leaves extraction and FeCl2 as precursors, as depicted in **Scheme 5**. Initially, the Ananas comosus leaves were carefully cut into pieces and immersed in dimethylformamide (DMF), followed by tip-sonication to extract the desired components. The resulting DMF extract obtained from the leaves serves as the

precursor, providing essential carbon and nitrogen sources, as well as acting as a metal protection agent[68]. Ananas comosus leaves are known to contain glucose and other polyphenol species, which serve as crucial carbon sources for the formation of graphene quantum dots. Additionally, these components play a significant role in preventing the aggregation of Fe2+ ions through chelation, thanks to the strong interaction between oxygen-containing and phenolic groups with metal ions[69]. To disperse the ferrous ions, iron(II) chloride was added to the DMF extract, and the mixture was subjected to 30 minutes of sonication in a water bath. Subsequent centrifugation was carried out to eliminate any large insoluble particles, and the resulting solution was then transferred to a Teflon reactor. The reaction mixture was subjected to a temperature of 190°C for 8 hours, allowing for the controlled synthesis of FeN/GQDs. The as-prepared FeN/GQDs nanozyme was then purified using a combination of centrifugation and dialysis to remove any impurities and unreacted precursors.

To assess the colloidal stability of the purified FeN/GQDs nanozymes, their hydrated size and zeta potential changes over time in PBS buffer solution were measured using Dynamic Light Scattering (DLS). As depicted in **Figure 1a**, the GQD-based nanozymes exhibited a consistently uniform hydrated size of approximately 11.6 (±2.3) nm, with a low polydispersity index (PDI) value of 0.122 (±0.05). The zeta potential of FeN/GQDs was measured to be 39.4 (±5.7) mV, indicating a favorable and stable colloidal system[70].

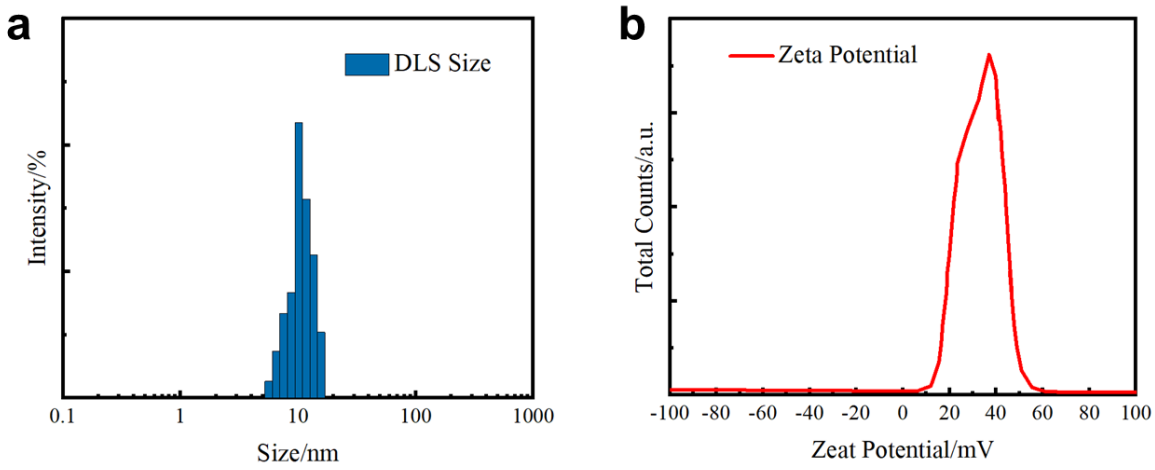

Figure 1. DLS size and zeta potential of FeN/GQDs

Transmission Electron Microscopy (TEM) was employed to provide further insights into the morphology and structural characteristics of the FeN/GQDs nanozymes. The TEM images revealed that the FeN/GQDs were evenly distributed in a spherical shape, exhibiting a well-dispersed nature with an average size of 10.6 (±2.7) nm **(Figure 2a**). The high-resolution TEM image confirmed the excellent crystallinity of the FeN/GQDs, displaying an ordered fringe pattern. The lattice interval of FeN/GQDs, determined to be 0.3 nm (**Figure 2b**), corresponds to the interlayer spacing of the [100] facet of sp2 graphitic carbon, further confirming the presence of graphene-like structures. The selected area electron diffraction (SAED) pattern shown in **Figure 2C** exhibited ring-like features, indicating the predominance of a graphene structure within the FeN/GQDs[71]. Moreover, TEM-X-ray energy-dispersive spectrometer (EDS) mapping was performed to verify the homogeneous distribution of carbon (**Figure 1d**), nitrogen (**Figure 1e**), and iron (**Figure 1f**) elements within the FeN/GQDs. These elements were found to be uniformly distributed throughout the nanozymes, as confirmed by the EDS mapping analysis. The high degree of crystallinity of FeN/GQDs was further substantiated.

The exceptional crystallinity of the FeN/GQDs nanozymes was corroborated through Raman spectroscopy analysis. Raman spectra were recorded to examine the characteristic vibrational modes of carbon within the nanozymes, spanning the 1000-2000 cm-1 region. Two prominent peaks were observed at 1358 cm-1 and 1613 cm-1, corresponding to the D-band and G-band, respectively. The D-band primarily arises from sp3 hybridized amorphous carbon structures, while the G-band originates from sp2 hybridized graphitic carbon networks, indicating the presence of well-structured graphene-based materials in the FeN/GQDs [72]. The intensity ratio of the D-band to G-band (0.32/0.91), as depicted in **Figure 3a**, further emphasized the highly crystalline nature of the FeN/GQDs. This ratio serves as a measure of the degree of graphitic carbon crystallinity, with a lower D-band intensity relative to the G-band indicating enhanced crystallinity. The FeN/GQDs exhibited a favorable ratio,

underscoring their highly crystallized structure. [73].

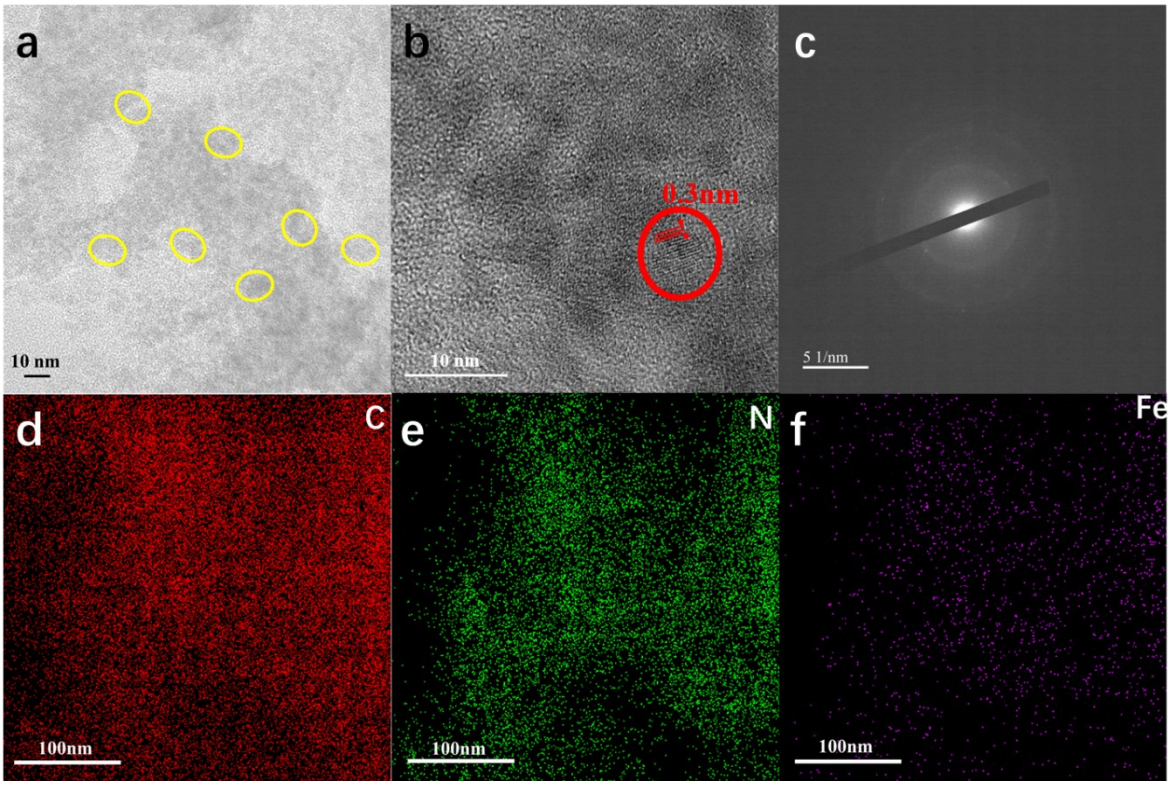

Figure 2. a). TEM image of FeN/GQDs with scale bar of nm; b). HRTEM image with scale bar; c). SEAD pattern of FeN/GQDs; d), corresponding EDS element mapping of FeN/GQDs

To explore the potential applications of FeN/GQDs in biosensing and other fields, a thorough investigation of their optical properties was conducted using UV-vis and fluorescence spectroscopy (**Figure 3b, c**). The UV-vis absorption spectrum of FeN/GQDs exhibited a characteristic absorption peak centered around 370 nm, attributed to the Π-Π* transition of the graphitic sp2 domains commonly observed in graphene-based materials. Notably, two distinct peaks were observed at approximately 670 nm and 850 nm, specifically in the near-infrared (NIR) regions I and II, respectively. It is particularly noteworthy that no significant absorption peaks were detected in the visible light region, which mitigates potential interference with commonly used substrate absorption peaks for biosensing applications. Fluorescence spectroscopy analysis of FeN/GQDs unveiled a remarkable fluorescence emission maximum at 750 nm when excited at 600 nm, resulting in a substantial Stokes shift of 150 nm (Figure

2c). This pronounced Stokes shift can be attributed to several factors. Firstly, the stacked aromatic carbon structures derived from the polyphenol precursors, as previously reported, contribute to the observed large Stokes shift. Furthermore, the incorporation of nitrogen into the graphene quantum dots induces a modification in the band structure of the nanoparticles. This alteration in the band structure, stemming from the Fe-N doping, further enhances the observed Stokes shift. The combined effect of these factors underscores the unique fluorescence properties of FeN/GQDs, particularly their emission in the near-infrared range.

The comprehensive characterization of FeN/GQDs included the analysis of their chemical composition using Fourier-transform infrared spectroscopy (FTIR) and X-ray photoelectron spectroscopy (XPS). The FTIR spectra of FeN/GQDs (**Figure 3d**) revealed the presence of a significant number of oxygen and nitrogen-containing functional groups on the surface of the graphene quantum dots. These functional groups were identified as -COOH, as indicated by the C=O stretching in the range of 1760-1690 cm-1 and the C-O stretching in the range of 1320-1210 cm-1[74]. The presence of -OH groups was observed through the O-H stretching in the range of 3300-2500 cm-1, as well as the O-H bending in the range of 1440-1395 cm-1 and 950-910 cm-1[74]. Furthermore, the presence of -NH2 groups was confirmed by the N-H stretching in the range of 3400-3250 cm-1, N-H bending in the range of 1650-1580 cm-1, C-N stretching (aromatic amines) in the range of 1335-1250 cm-1, and N-H wagging from 910-665 cm-1[74]. Notably, peaks corresponding to Fe-O bonds around 680, 520, and 440 cm-1 were barely detected in the FeN/GQDs sample, suggesting a minimal presence of Fe-O species[75]. To further investigate the surface elements and their binding states, XPS analysis was performed. The full survey XPS spectrum of FeN/GQDs (**Figure 4a**) confirmed the presence of characteristic peaks corresponding to carbon (C(1s)), oxygen (O(1s)), nitrogen (N(1s)), and iron (Fe(2p3/2,2p1/2)). The binding energy peaks observed were located at approximately 285, 531, 400, and 710 eV, respectively. The high-resolution XPS spectra were employed to analyze the binding structures of carbon and nitrogen. The C1s spectrum (**Figure 4b**) exhibited three well-defined peaks

at 285 eV, 287 eV, and 289 eV, which were assigned to sp2 carbon, O-C=O, and C=N, respectively. The N1s spectrum **(Figure 4c)** displayed four distinct peaks, indicating the coexistence of Pyridinic-N (Fe-N), graphitic-N, Pyrrolic-N, and Oxidized-N[76]. Previous studies have suggested that the presence of pyridinic and pyrrolic nitrogen can form coordination bonds with Fe, resulting in the formation of Fe-Nx structural units[76]. This finding is further supported by the analysis of the Fe2p spectra (**Figure 4d**). The first doublet of Fe2+2p3/2 (711.2 eV) and Fe2+2p1/2 (725.3 eV) confirms the presence of Fe2+ in the FeN/GQDs, while the peaks located at 717.3 eV and 731.7 eV can be attributed to the satellite signals of Fe-Nx and Fe-O, respectively[77]. Based on the above data, it can be concluded that Fe single atoms were successfully doped into the graphene quantum dots through the Fe-Nx coordination structure. This finding highlights the potential of FeN/GQDs as highly efficient catalysts for various chemical reactions, owing to their unique chemical composition and structure.

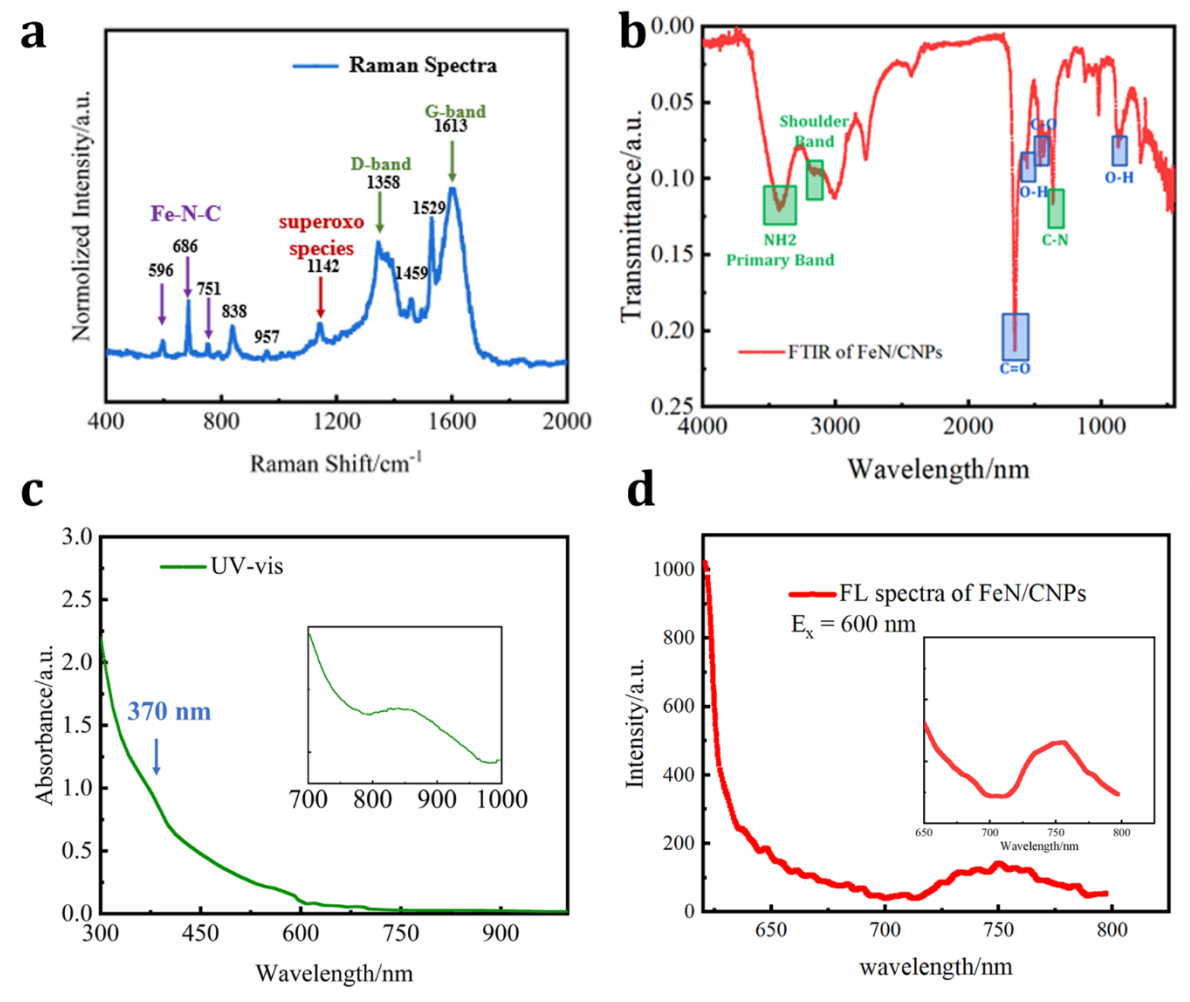

Figure 3. Physicochemical characterization of FeN/GQDS. a). and b). Raman spectra of FeN/GQDs with different chemical shift regions; c). FL spectra of FeN/GQDs with a Excitation wavelength at 600nm; d). FT-IR spectra of FeN/GQDs; e) and f), XPS N1s and XPS Fe2p spectra of FeN/GQDs.

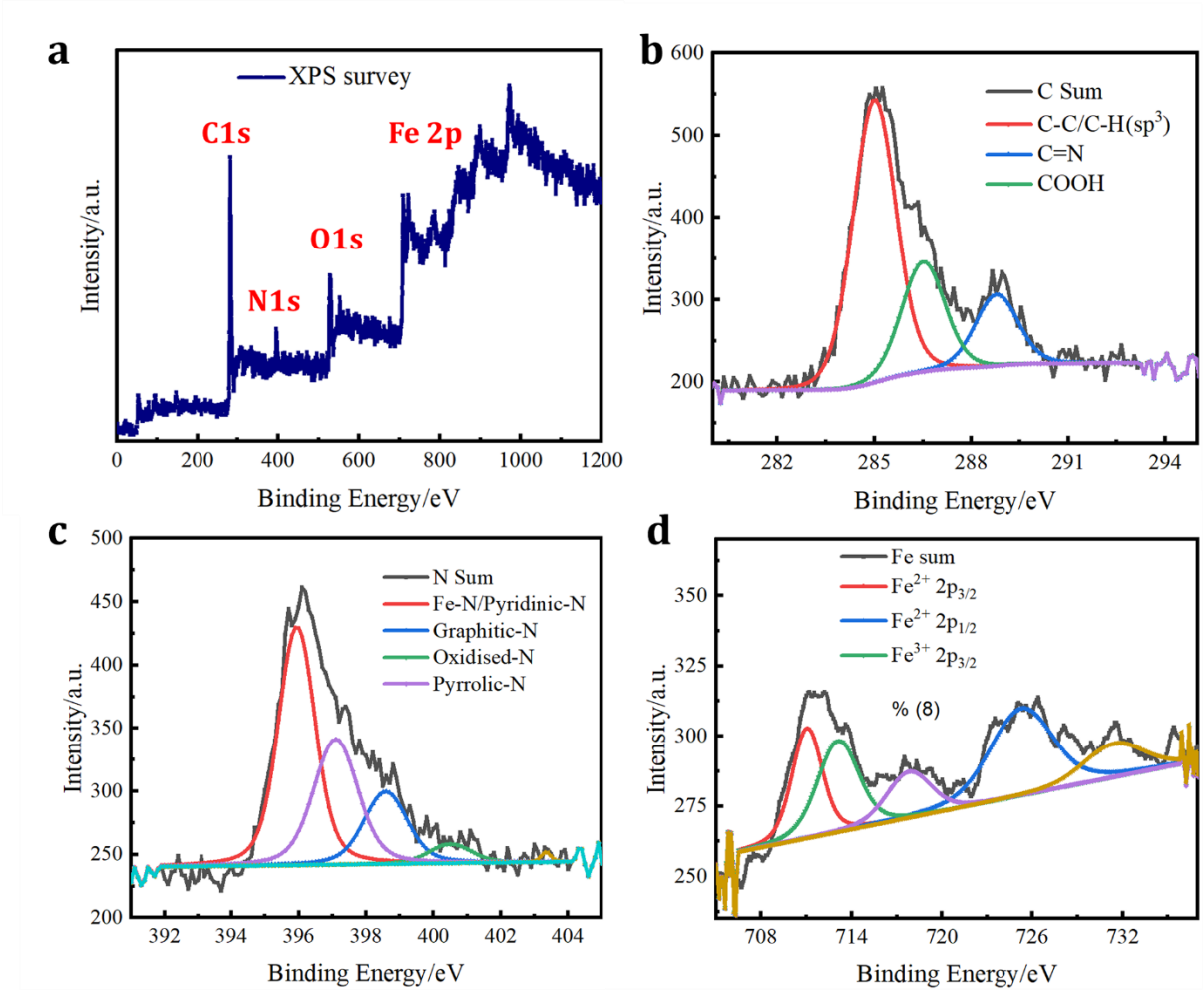

Figure 4. XPS spectra of FeN/GQDs. a) XPS survey, b) Carbon, c) Nitrogen, d) Iron

In order to explore the atomic structure of FeN/GQDs nanozymes, the coordination environment and chemical state of Fe species were thoroughly investigated using X-ray absorption near edge structure (XANES) and extended X-ray absorption fine structure (EXAFS) spectroscopy were performed at the Fe K edge to investigate the structural properties of FeN/GQDs (**Figure 5**). The XANES spectra (**Figure 5a**) demonstrated that the absorption energy of FeN/GQDs was intermediate between that of the Fe foil and Fe_2O_3, suggesting the existence of positively charged Fe single atoms in the nanozymes. This observation suggests that the Fe atoms within FeN/GQDs are in a distinct chemical state compared to metallic iron or iron oxide. Further analysis of the EXAFS curve of FeN/GQDs exhibited a prominent peak at approximately 1.5 Å, which was assigned to the Fe-N scattering paths (Figure 4b). Importantly, there is no significant peak corresponding to Fe-Fe bonding at 2.2 Å

was detected in the EXAFS spectrum. This finding indicates the absence of Fe-Fe interactions within the atomic structure of FeN/GQDs, further supporting the presence of individual Fe atoms. By analyzing the EXAFS fitting parameters (**Table 2**), an average Fe-N coordination number of 4.6 was determined, providing quantitative evidence for the coordination environment of Fe atoms within the nanozymes.

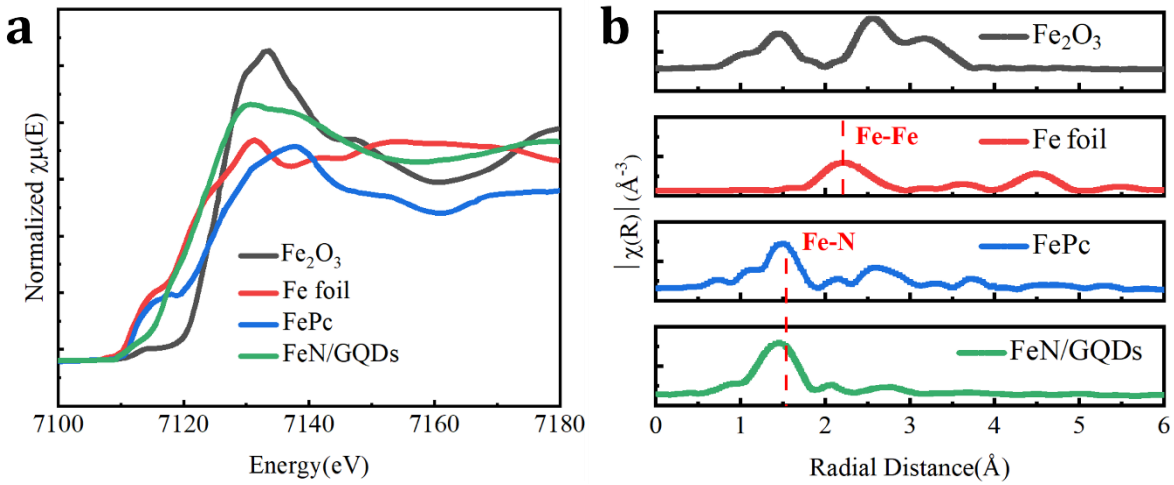

Figure 5. Atomic structural analysis of FeN/GQDs by XANES and EXAFS.

Table 2. EXAFS data fitting results of FeN/GQDs. (S0 2 =0.75)

Sample	Path	CN	R(Å)	σ 2 (10 -3 Å 2)	ΔE 0 (eV)	R-factor
FeN/GQDs	Fe-N	4.6	2.04	6.6	2.3	0.01

Based on the combined analysis of XANES and EXAFS, it can be confidently concluded that FeN/GQDs contain isolated Fe atoms as evidenced by the absence of Fe-Fe bonding interactions and the presence of Fe-N scattering paths. The unique atomic structure of FeN/GQDs, with positively charged Fe single atoms coordinated to nitrogen, contributes to their exceptional catalytic properties and makes them highly promising for a wide range of applications in catalysis, sensing, and other fields.

2. Peroxidase-like activity and kinetics analysis

Peroxidase (POD) is a natural enzyme that plays a critical role in many biological processes by catalyzing the decomposition of hydrogen peroxide into water and ROS[78]. In our study, we evaluated the POD-like activity

of the Fe-N/GQDs nanozymes using a commonly used chromogenic substrate, TMB, which can be converted into a blue-colored TMB product (oxTMB) with a typical absorbance peak around 652 nm when combined with -OH free radicals generated by the nanozymes, as shown in Equation 2:

$$TMB + H_2O_2 \rightarrow oxTMB + H_2O \quad \text{(Equation 2)}$$

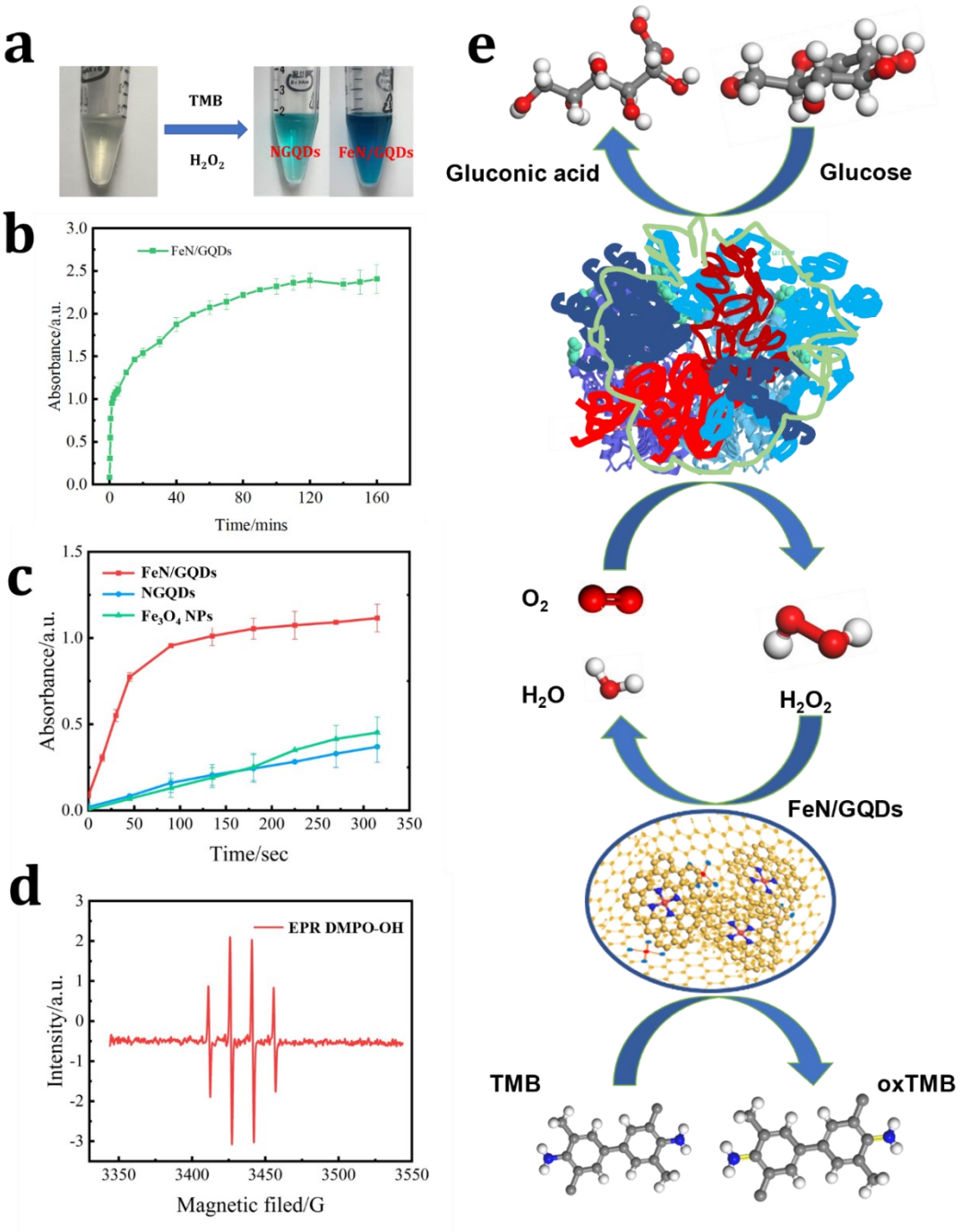

Figure 6. Peroxidase-like activity and kinetics analysis of FeN/GQDs. a). Nanozymes show peroxidase-like activity by catalyzing the substrates (TMB, DAB and OPD) to produce colorimetric reactions; b). Reaction-time curves of the TMB

colorimetric reaction

Figure 6a demonstrates a time-dependent increase in absorbance upon the addition of H2O2 to the FeN/GQDs/TMB solution. To accurately capture the optimal reaction kinetics, absorbance values were specifically recorded at the 6th minute for further analysis. This time point was chosen as beyond it, the slope of absorbance with respect to time gradually diminishes. In order to effectively illustrate the impact of the Fe-N coordination structure on the POD-like activity, the relative catalytic efficiencies of various nanozymes, including FeN/GQDs, NGQDs, and Fe3O4 nanoparticles, were compared by monitoring the color change of the solution and the absorbance at 652 nm over time. The results conclusively indicate that the catalytic efficiency of FeN/GQDs surpasses that of both NGQDs and Fe2O3 nanoparticles, as observed by the naked eye and the absorbance at 652 nm. (**Figure 6b, c**)

The reaction efficiency of the catalytic process primarily relies on the production of superoxide radicals (-OH, -OOH). To confirm the generation of reactive oxidative species (ROS) such as -OH and -OOH in the catalytic reaction system of FeN/GQDs, the EPR spin-trap technique using DMPO conjugation was employed (**Figure 6d**). The EPR spectra showed a distinctive 1:2:2:1 signal pattern of -OH in the sample containing both H2O2 and FeN/GQDs, indicating the presence of -OH radicals. This signal pattern was not observed in samples without nanozymes or H2O2, further supporting the involvement of FeN/GQDs in the generation of -OH radicals.

To find the most optimized reaction condition, the pH environment and temperature effect are investigated separately. The result shows a best pH environment value as 3.6 among pH 2 to 10 (**Figure. 7a**) and a best temperature as 30 ℃ (**Figure. 7b**) from 17 to 60 ℃. Besides, the relationship between the reaction efficiency and chemical reagent dosage are also surveyed (**Figure. 7c, d**), the result shows that the reaction efficiency is positively correlated with the dosage of H2O2, TMB and nanozymes.

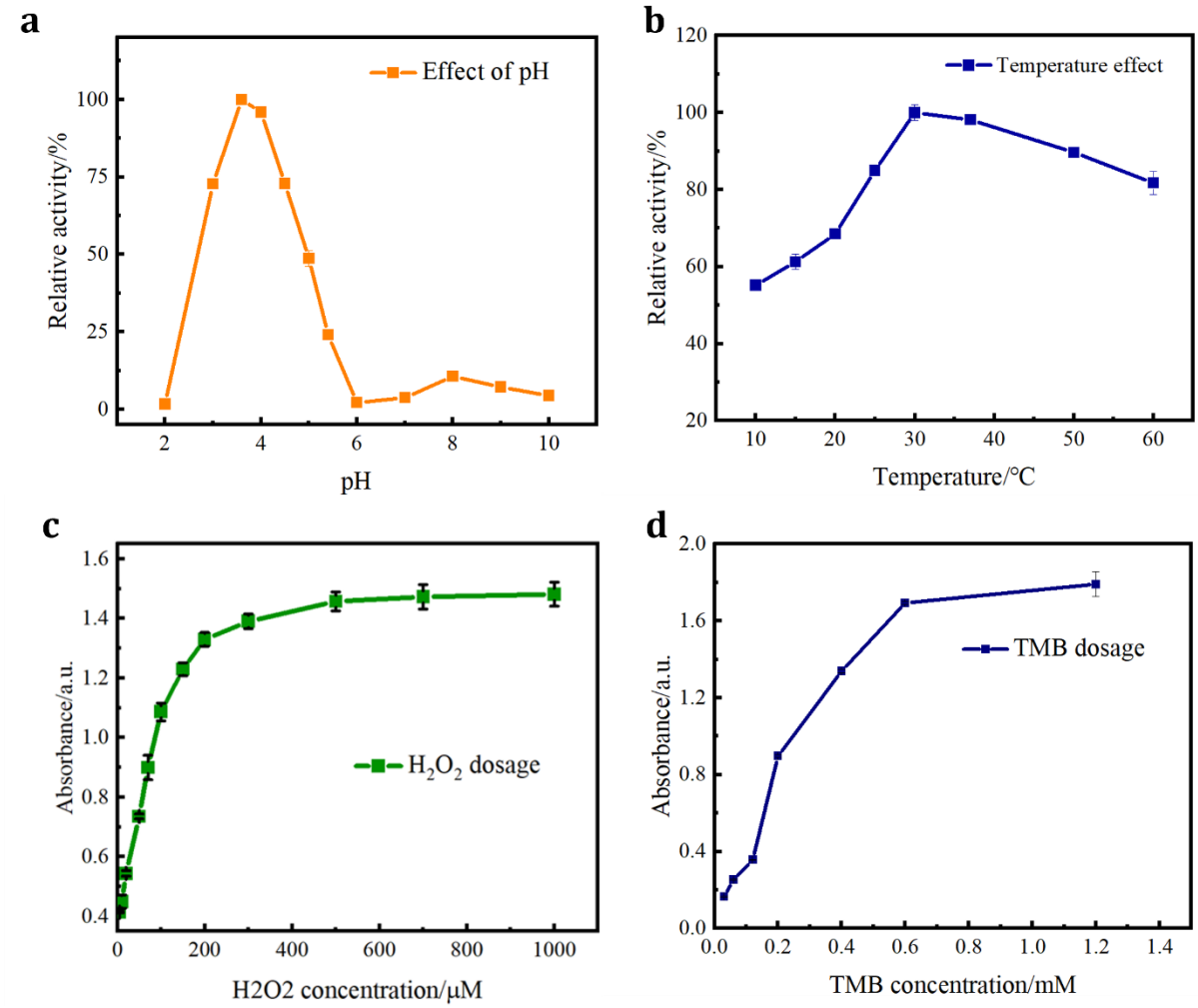

Figure 7. The influence of reaction conditions on the peroxidase-like activity of FeN/GQDs. a). different pH environment (pH2-10), b). Temperature effect (17-60℃), c) H2O2 dosage, and d) TMB dosage.

In order to gain further insights into the peroxidase-like activity of FeN/GQDs, the steady-state kinetics were investigated by varying the concentrations of H2O2 or TMB (**Figure 8a, b**). The Lineweaver-Burk or double reciprocal plots were utilized to analyze the data and determine the Michaelis constant (Km) and maximal reaction velocity (Vmax) (**Figure 8c, d**). The Km value represents the binding capacity between the enzyme and its substrates, with a lower value indicating a stronger affinity. For FeN/GQDs, the Km values were determined to be 0.52 for TMB and 0.49 for H2O2, respectively. In order to further elucidate the excellent performance of FeN/GQDs, different types of nanozymes were selected for a complete comparison of reaction constants. The results shows that the km for H2O2 of FeN/GQDs is 7.5 times lower than that of HRP, which suggesting the superior capacity for activating H2O2. Besides, for Vmax, FeN/GQDs shows a higher catalytic ability, 10 times

higher than that of HRP. Moreover, compared to other recent reported nanoz

ymes (**Table 3**), FeN/GQDs shows much lower Km value and higher Vmax, which suggests that FeN/GQDs exhibits higher peroxidase mimic.

Table 3. Comparison of the kinetic parameters (V_{max} and K_m values) s of FeN/GQDs with other nanozymes.

Materials	Substrate	K_m(mM)	V_{max}($M^{-1}S^{-1}$)
FeN/GQDs[a]	TMB	0.52	$6.37*10^{-6}$
	H_2O_2	0.49	$8.32*10^{-6}$
Fe_3O_4[79]	TMB	31.2	$1.614*10^{-6}$
	H_2O_2	2.995	$0.9193*10^{-6}$
FeSSN[32]	TMB	0.53	$2.04*10^{-7}$
	H_2O_2	0.36	$1.32*10^{-7}$
Fe-N-C[56]	TMB	3.6	$3.56*10^{-7}$
	H_2O_2	12.2	$8.60*10^{-8}$
Fe3O4@Cu/GMP–Gox[80]	TMB	15.37	$9.06*10^{-8}$
	H_2O_2	6.35	$3.85*10^{-8}$
g-C3N4/PdNPs/ Fe3O4NPs[81]	TMB	1.05	$9.58*10^{-6}$
	H_2O_2	7.71	$1.26*10^{-5}$
Fe-Sazyme[82]	TMB	0.3	$18.35*10^{-8}$
	H_2O_2	0.21	$9.94*10^{-8}$
Fe3O4[46]	TMB	530	$3.44*10^{-8}$
	H_2O_2	8.8	$9.78*10^{-8}$
HRP[46]	TMB	0.434	$1.00*10^{-7}$
	H_2O_2	3.7	$8.71*10^{-8}$

[a]: This work

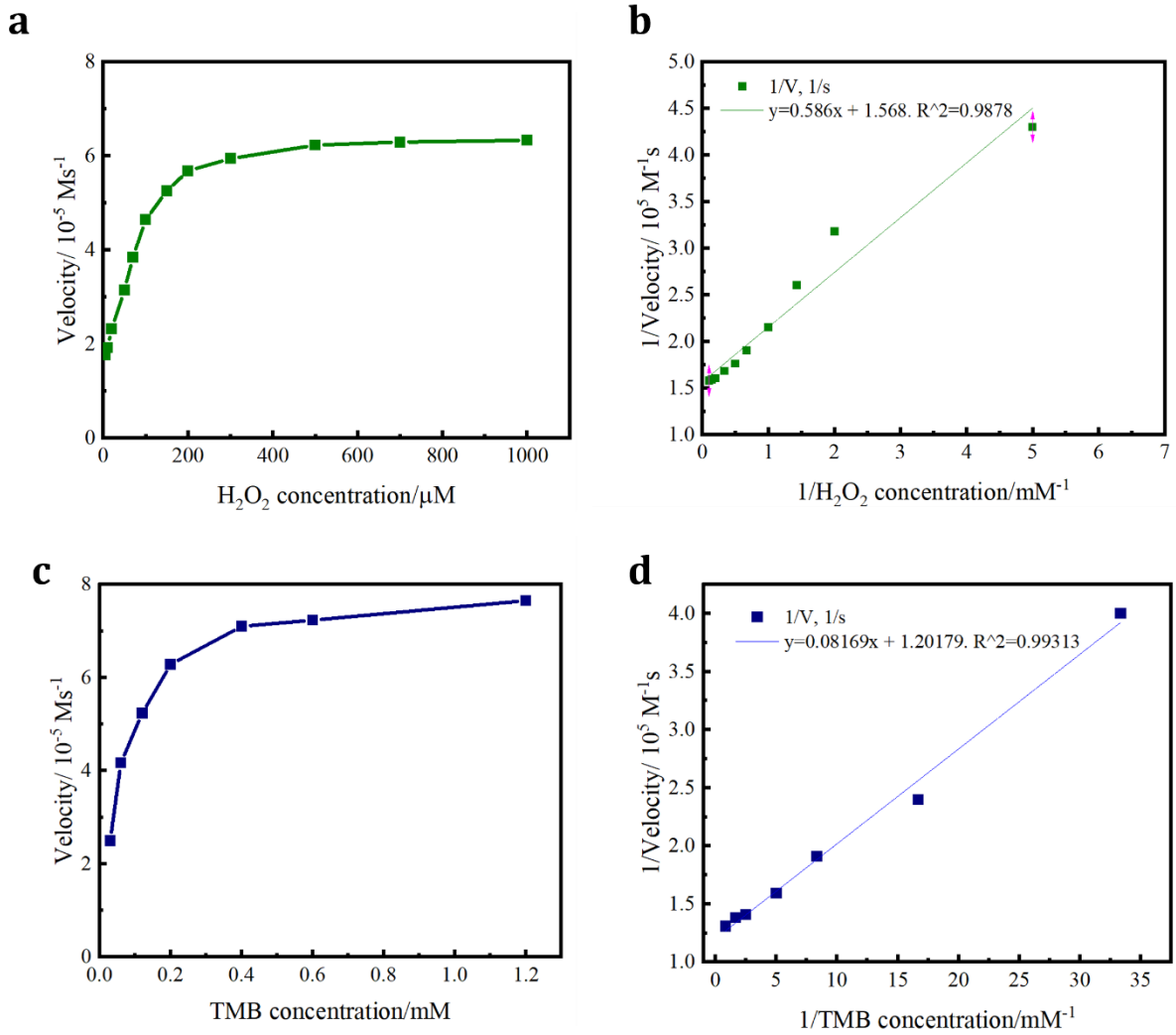

Figure 8. The steady state kinetic analysis for FeOx@SHS-500 under various conditions. (a) [TMB] = 0.4 mM; [H2O2]=5-100μM, (c) [H2O2]=10μM; [TMB] = 0.05-1.2 mM; (b) and (d) are the Lineweaver-Burk double reciprocal plots corresponding to conditions (a) and (c). The reaction was carried out with 10 μg/mL catalyst of 0.1 M Hac-NaAc buffer, pH=3.6, and temperature=37 °C

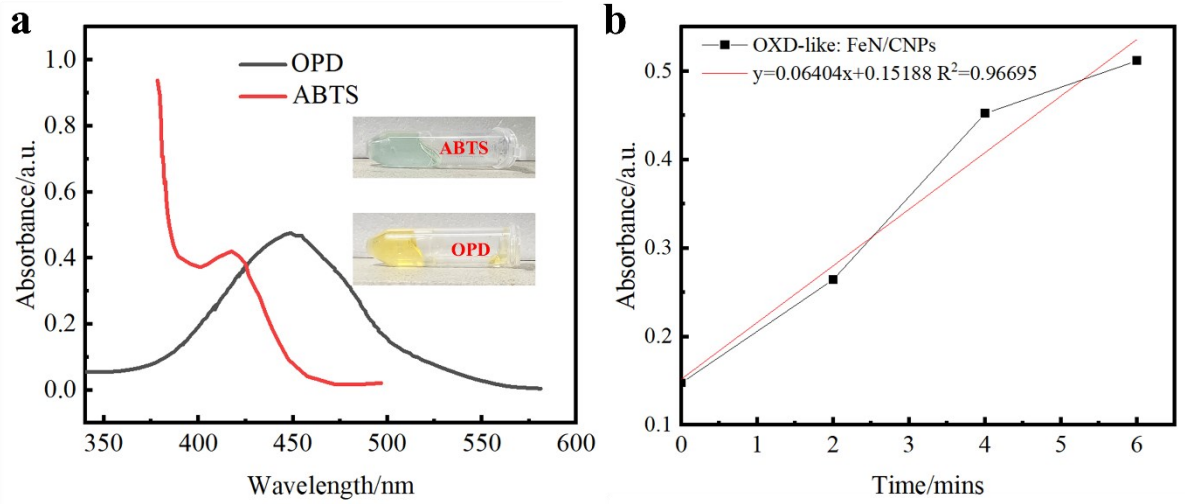

Figure 9. UV-visible spectra showing oxidation of OPD and ABTS using FeN/GQDs nanozymes.

Moreover, FeN/GQDs exhibit remarkable versatility as a nanozyme, demonstrating peroxidase-like activity with various chromogenic substrates. In addition to TMB, ABTS and OPD (**Figure 9a**) can also be effectively oxidized by FeN/GQDs, leading to distinct color changes (green and orange) in the catalytic system. This highlights the broad catalytic capability of FeN/GQDs towards different chromogenic substrates. Furthermore, the superoxide dismutase-like activities of FeN/GQDs nanozymes were investigated (**Figure 9b**). Although the catalytic parameters are lower than those of natural enzymes, the results demonstrate the catalytic specificity of FeN/GQDs. These properties significantly expand the potential applications of FeN/GQDs as a versatile candidate for colorimetric detection in various fields.

3. Glucose detection performance evaluation of FeN/GQDs

To utilize the enhanced peroxidase-like activity of FeN/GQDs, a colorimetric glucose sensing system was developed. The system involved a mixture of glucose oxidase (GOx) enzyme and the colorimetric substrate, TMB. The detection process relied on cascade reactions (**Figure 5e**). Initially, glucose was oxidized by GOx enzyme, leading to the production of hydrogen peroxide (H2O2). Then, the FeN/GQDs nanozyme catalyzed the conversion of H2O2 to hydroxyl radicals (-OH). These hydroxyl radicals, in turn, oxidized the initially colorless TMB substrate, resulting in the formation of a blue-colored product called oxTMB. The levels of produced H2O2 and glucose were determined by monitoring the changes in the intensity of the UV-vis absorption peak at 652 nm corresponding to oxTMB. The color response was evaluated by adding H2O2 and glucose under the optimized conditions for FeN/GQDs nanozyme.

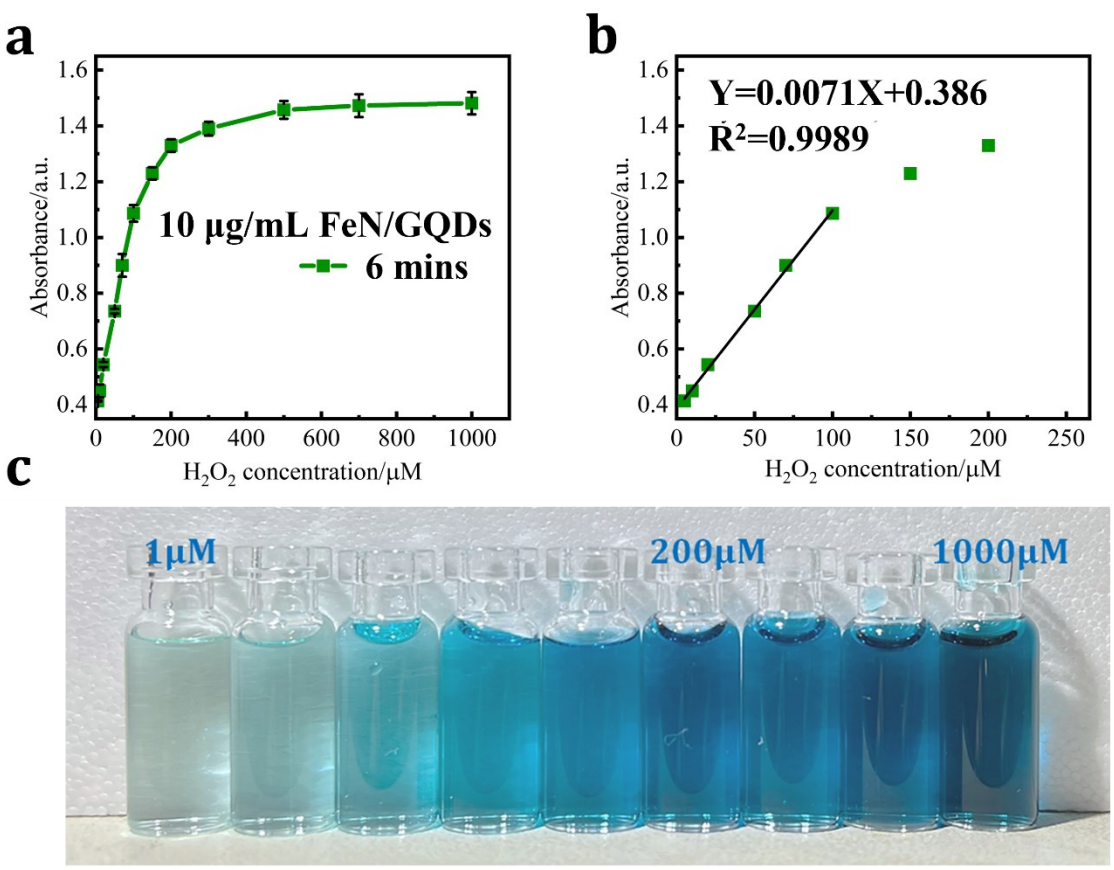

Figure 10. The result of TMB assay with H2O2 as substrate, the final concentration of each component are FeN-CNPs: 10ug/mL, TMB: 0.3mM, and with 1mM pH3.6 PBS buffer. a) The absorbance change with H2O2 concentration increased. b) Over the 99% confidence.

Based on the excellent POD-like enzyme catalytic performance of FeN/GQDs, the linear relationship between H2O2 concentration of substrate and ROS production is first analyzed to find 99% confidence intervals. As shown in **Figure 10a**, with the increase of H2O2 concentration, its absorbance gradually reaches saturation. A linear correlation was observed in the concentration range of 5-100 μM for H2O2, as demonstrated by the concentration-response plot in **Figure 10b**. Figure.6c shows the color change of H2O2/TMB/FeN-GQDs solution with different H2O2 concentration. Different shades of blue can be observed based on the H2O2 concentrations, with a deeper blue color indicating higher H2O2 concentrations in the detection system. When the concentration reached 200μM, the color hardly changed, which was consistent with Figure. 6a, that is because the dosage of FeN/GQDs, 10μg/mL was very low, and its ROS catalytic activity reached saturation. Finally, the detection limit

of H2O2 is calculated to be 0.78 μM. In a typically cascade reaction for glucose detection, H2O2 is the product of glucose, which indicates that the detection limit of glucose can be lower than 0.78 μM.

To further investigate the detection capability of FeN/GQDs towards glucose, we employed UV-Vis to measure absorbance increase of glucose solutions at 652nm with glucose concentrations ranging from 1 μM to 1000 μM (**Figure 11a**). The glucose solution first reacts with the glucose oxidase (GOx), and 30 minutes after the 36°C-water bath, it was added into the TMB/FeN/GQDs solution. The glucose/GOx/TMB/FeN/GQDs solution could show a quick response within 6 mins upon the mixture (**Figure 11c**). Its absorbance increases with the glucose concentration, which is because H2O2 is generated after the reaction of glucose and GOx, and H2O2 production is positively correlated with glucose concentration. At the same time, the color range of the system has a very good linear relationship in the range of 1 μM to 300 μM (**Figure. 11b**). The detection limit was determined to be 0.36 μM by a relative standard deviation of 0.83%.

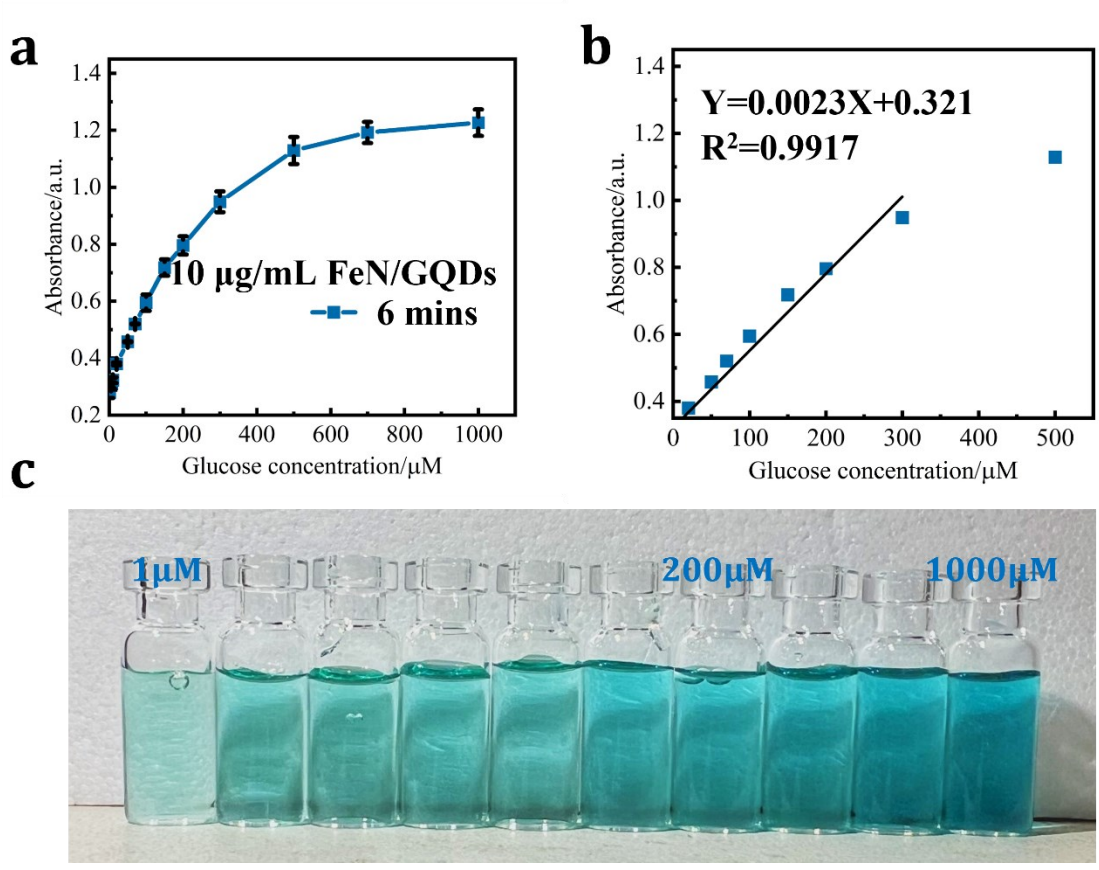

Figure 11. The result of TMB assay for glucose detection, the final concentration of each component are: FeN-CNPs: 10ug/mL,

TMB: 0.3mM, Glucose oxides (GOx): 0.25mg/mL, and with 1mM pH3.6 PBS buffer. a) The absorbance changes at 652 nm with glucose concentration increased. b) Over the 99% confidence interval, the increase in glucose concentration as a function of the increase in absorbance: glucose concentration from 5μM to 100μM. c) the color change of glucose/GOx/TMB/FeN-CNPs with the increases of glucose concentration.

Compared to other glucose detection systems utilizing Iron based nanozymes (**Table S**4), our system exhibited outstanding catalytic performance, offering a broad detection range and remarkable sensitivity. Moreover, FeN/GQDs not only offers a lower detection limit but also enables rapid testing, with results obtained within 6 minutes. This significant improvement in both time and accuracy enhances the overall performance of the glucose detection system. Although this nanozyme glucose detection system is based on the cascade process, rather than direct detection, these data demonstrate that FeN/GQDs with highly dispersed active sites brought by unique Fe-N structure have extremely high reactivity and stability, which can be applied in a variety of biomedical applications.

Table S4. Comparison of glucose detection performance with different nanozymes: detection range, detection limits, and detection time.

Nanozymes	Detection Method	Detection Range	Detection Limits	Assay Time
Au NPs/Ag NPs[83]	CM*	5–70 μM	3 μM	40 min
Au@BSA NPs[84]	CM	1–300 μM	0.6 μm	30 min
Au@PNIPAm[77]	CM	10-70 mM	5.07 mM	20 min
Cu-Pt bimetallic fabrics[85]	CM	1–12.5 mM	0.84 mM	5 min
GO/AuNPs[86]	CM	2-30 μM	0.473 μM	60 min
PtNZs[87]	CM	10–1000μM	3.9uM	15 min
Fe-MOF-Gox[88]	CM	1–500 μM	0.487 μM	30 min
Fe3O4 NPs[89]	CM	0.05–4 mM		10 min
Au (BiSA@Au)[90]	CM	80 -1000 μM	43.2 μM	30 min

g-C3N4@CuMOFs[91]	FM**	0.1-22 μM	0.059 μM	30 min
Ag@AuNPs–GO[92]	SERS	2–6 mM	0.33 mM	15 min
Bimetallic film over nanospheres[93]	SERS	0.1–10 mM	0.1 mM	60 min
AgNP/PATP–PMBA[94]	SERS	0.5–10 mM	0.03mM	180 min
GOD/AuNPs/GO/GFME[95]	CV	10-15μM	1.2 μM	/
Gox-PABA-gFETs[96]	CV	10-1000 μM	4.1 μM	/
rGO/Cu–Cu2O[97]	CV	0.01-7uM	0.06uM	/
FeN/GQDs***	CM	1-100uM	0.78uM	6 min

*: Colorimetric

**: Fluorometric

***: This work.

4. Stability and reusability of FeN/GQDs nanozymes

Stability and reusability, as critical indicators for the practical application of nanozymes, have been further investigated in this study. The nanozymes were subjected to storage at room temperature for 30 days to assess their particle dispersion and catalytic activity. The analysis of particle size distribution and polydispersity index (PDI) by DLS revealed that the nanozymes exhibited exceptional colloidal stability even after the 30-day storage period (**Figure 12a**). Additionally, the TMB experiment demonstrated that the catalytic activity of the nanozymes remained largely unaffected, confirming their remarkable stability (**Figure 12b**). The results underscore the structural integrity and functional reliability of FeN/GQDs nanozymes over an extended duration. To evaluate the reusability of the nanozymes, a recycling experiment was conducted. The post-TMB reaction nanozymes were collected and washed through an ultrafiltration membrane. Subsequently, the washed nanozymes were subjected to a TMB assay to assess their catalytic activity. Notably, as shown in **Figure 12c**, the catalytic performance of the washed nanozymes retaining approximately 98.2% of their initial catalytic activity, indicating their impressive

reusability. This signifies that FeN/GQDs nanozymes can be efficiently recovered and employed for subsequent catalytic reactions without significant loss in their catalytic performance. However, it should be noted that a significant decrease in catalytic activity (89.6%) was observed after the second washing. This decline can be attributed to the substantial loss of nanozymes during the washing process. The results obtained from the stability and reusability experiments validate the long-term stability and functionality of FeN/GQDs nanozymes, positioning them as promising candidates for a wide range of catalytic applications.

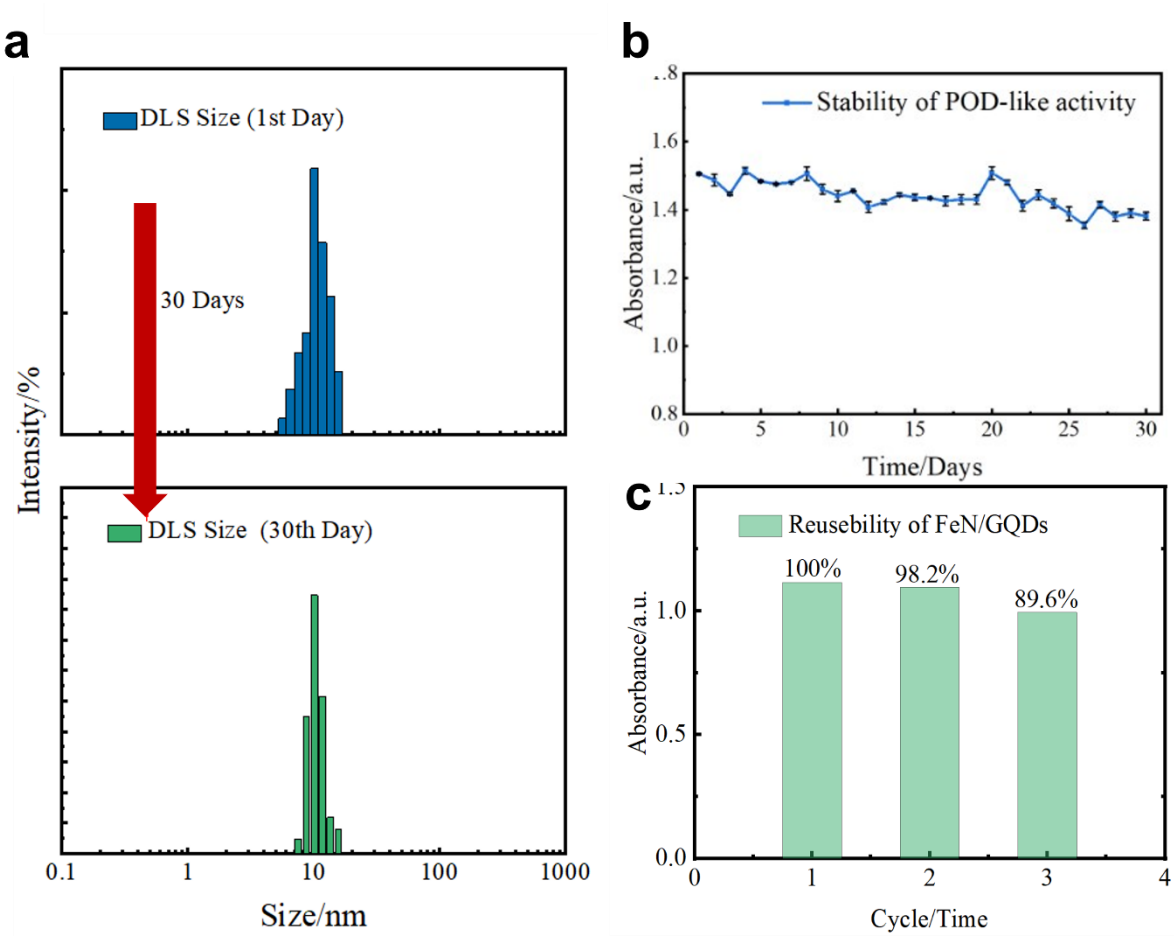

Figure 12. Stability and reusability of FeN/GQDs nanozymes. a). colloidal stability of FeN/GQDs, store under room temperature for 30 days. b). Changes in absorbance of TMB assay with FeN/GQDs for 30 days, c). Reusability of FeN/GQDs after purification.

Chapter 7. Conclusion and Future Work

In conclusion, the study successfully synthesized single Fe atom nanozymes using a green synthesis method via a simple hydrothermal process, which is not only simple and cost-effective but also eco-friendly. XANES analysis

confirmed the presence of single Fe atoms in the nanozymes, and further investigations using TEM and XPS provided additional evidence for the unique structure and composition of the nanoparticles. EPR spectroscopy characterized the POD-like activity of the Fe atom nanozymes, revealing a clear POD-like signal. The glucose detection assay demonstrated that the Fe atom nanozymes exhibit excellent sensitivity and selectivity for glucose detection, with a detection limit as low as 0.36 μM and a linear range up to 300uM. The high catalytic activity of the nanozymes is attributed to the single Fe atom structure, which provides a large number of active sites for glucose oxidation. Moreover, the combination of the NIR emission and high POD-like activity suggests that these nanozymes have significant potential for clinical applications, such as photodynamic therapy, bioimaging, and biosensing. In summary, the study provides a new approach for synthesizing single atom nanozymes with excellent properties, which has significant implications for the development of advanced nanomaterials for biosensing and medical applications.

In terms of the further development of FeN/GQDs nanozymes, there are two main directions. First, it is necessary to overcome the problem of instability of FeN/GQDs in neutral or alkaline solutions for further in-vitro/vivo studies. Considering about the FTIR data, there are certain mount of $-NH_2$ group on the nanozymes surface, which can prevent the aggregation when there is excess H^+ in the solution. However, when the solution is neutral or alkaline, the concentration of H^+ are greatly decreased, then, the FeN/GQDs cannot maintain the colloidal stability. One potential approach, which is also the most commonly used method is to conjugate the polymer through PEGylation. However, the widely used coupling agents, EDC/NHS, are not easily applicable to this nanozyme due to the presence of abundant amino functional groups, which can lead to cross-linking between the nanozymes after the formation of EDS intermediates. Therefore, further research is needed to explore and determine suitable approaches for the conjugation of FeN/GQDs. Second, a deeper understanding of the growth mechanism of single-atom nanozymes is necessary. As the hydrothermal synthesis method relies on self-assembly

processes, the synthesis conditions and precursor composition have a significant impact on the resulting nanostructure. Therefore, further research is needed to investigate and fine-tune the growth mechanism of single-atom nanozymes. This can be achieved by adjusting and precisely controlling the precursor composition, as well as the research about the Activation energy of reaction for those intermediate precursors.

References

[1] S. Cai, R.J.F.i.C. Yang, Two-dimensional nanomaterials with enzyme-like properties for biomedical applications, 8 (2020) 565940.

[2] J. He, P. Liu, R. Ran, W. Wang, W. Zhou, Z.J.J.o.M.C.A. Shao, Single-atom catalysts for high-efficiency photocatalytic and photoelectrochemical water splitting: Distinctive roles, unique fabrication methods and specific design strategies, 10 (2022) 6835-6871.

[3] H. Zhang, X.F. Lu, Z.-P. Wu, X.W.D.J.A.C.S. Lou, Emerging multifunctional single-atom catalysts/nanozymes, 6 (2020) 1288-1301.

[4] Q. Wang, L. Zhang, C. Shang, Z. Zhang, S.J.C.C. Dong, Triple-enzyme mimetic activity of nickel–palladium hollow nanoparticles and their application in colorimetric biosensing of glucose, 52 (2016) 5410-5413.

[5] Y. Zhang, W. Chen, M. Jing, S. Liu, J. Feng, H. Wu, Y. Zhou, X. Zhang, Z.J.C.E.J. Ma, Self-assembled mixed micelle loaded with natural pyrethrins as an intelligent nano-insecticide with a novel temperature-responsive release mode, 361 (2019) 1381-1391.

[6] Y. Hu, R. Wang, S. Wang, L. Ding, J. Li, Y. Luo, X. Wang, M. Shen, X. Shi, Multifunctional Fe3O4 @ Au core/shell nanostars: a unique platform for multimode imaging and photothermal therapy of tumors, Scientific Reports, 6 (2016) 28325.

[7] Z.-H. Li, Y. Chen, Y. Sun, X.-Z.J.A.n. Zhang, Platinum-doped prussian blue nanozymes for multiwavelength bioimaging guided photothermal therapy of tumor and anti-inflammation, 15 (2021) 5189-5200.

[8] Y.-J. Huang, H.-C. Chen, H.-K. Lin, K.-H.J.A.a.m. Wei, interfaces, Doping ZnO electron transport layers with MoS2 nanosheets enhances the efficiency of polymer solar cells, 10 (2018) 20196-20204.

[9] C. He, D. Liu, W.J.A.n. Lin, Self-assembled core–shell nanoparticles for combined chemotherapy and photodynamic therapy of resistant head and neck cancers, 9 (2015) 991-1003.

[10] F. Cao, L. Zhang, Y. You, L. Zheng, J. Ren, X.J.A.C. Qu, An enzyme-mimicking single-atom catalyst as an efficient multiple reactive oxygen and nitrogen species scavenger for sepsis management, 132 (2020) 5146-5153.

[11] Z. Wang, D.C.J.N.c. Baulcombe, Transposon age and non-CG methylation, 11 (2020) 1221.

[12] X. Zhang, X. Chen, Y. Zhao, Nanozymes: Versatile Platforms for Cancer Diagnosis and Therapy, Nano-Micro Letters, 14 (2022) 95.

[13] X. Zhang, S. Wang, G. Cheng, P. Yu, J.J.E. Chang, Light-responsive nanomaterials for cancer therapy, 13 (2022) 18-30.

[14] S. Huang, B. Wang, X. Zhang, F. Lu, Z. Wang, S. Tian, D. Li, J. Yang, F. Cao, L.J.B. Cheng, High-purity weight-bearing magnesium screw: translational application in the healing of femoral neck fracture, 238 (2020)

119829.
[15] L. Jiao, J. Wu, H. Zhong, Y. Zhang, W. Xu, Y. Wu, Y. Chen, H. Yan, Q. Zhang, W.J.A.C. Gu, Densely isolated FeN4 sites for peroxidase mimicking, 10 (2020) 6422-6429.
[16] S. Ahmadi, N. Rabiee, M. Bagherzadeh, F. Elmi, Y. Fatahi, F. Farjadian, N. Baheiraei, B. Nasseri, M. Rabiee, N.T.J.N.t. Dastjerd, Stimulus-responsive sequential release systems for drug and gene delivery, 34 (2020) 100914.
[17] Z. Pu, I.S. Amiinu, R. Cheng, P. Wang, C. Zhang, S. Mu, W. Zhao, F. Su, G. Zhang, S.J.N.-M.L. Liao, Single-atom catalysts for electrochemical hydrogen evolution reaction: recent advances and future perspectives, 12 (2020) 1-29.
[18] Y. Chao, L. Xu, C. Liang, L. Feng, J. Xu, Z. Dong, L. Tian, X. Yi, K. Yang, Z. Liu, Combined local immunostimulatory radioisotope therapy and systemic immune checkpoint blockade imparts potent antitumour responses, Nature Biomedical Engineering, 2 (2018) 611-621.
[19] S. Liu, H. Xu, D. Liu, H. Yu, F. Zhang, P. Zhang, R. Zhang, W.J.J.o.t.A.C.S. Liu, Identify the activity origin of Pt single-atom catalyst via atom-by-atom counting, 143 (2021) 15243-15249.
[20] R. Yan, S. Sun, J. Yang, W. Long, J. Wang, X. Mu, Q. Li, W. Hao, S. Zhang, H.J.A.n. Liu, Nanozyme-based bandage with single-atom catalysis for brain trauma, 13 (2019) 11552-11560.
[21] D. Wang, B. Zhang, H. Ding, D. Liu, J. Xiang, X.J. Gao, X. Chen, Z. Li, L. Yang, H.J.N.T. Duan, TiO2 supported single Ag atoms nanozyme for elimination of SARS-CoV2, 40 (2021) 101243.
[22] S. Dell'Elce, F. Liscio, A. Kovtun, S. Allegri, O.M. Roscioni, C. Albonetti, G. De Luca, H.W. Amenitsch, N. Demitri, L.J.N. Giorgini, 3D to 2D reorganization of silver–thiol nanostructures, triggered by solvent vapor annealing, 10 (2018) 23018-23026.
[23] H. Wang, Y. Wang, L. Lu, Q. Ma, R. Feng, S. Xu, T.D. James, L.J.A.F.M. Wang, Reducing Valence States of Co Active Sites in a Single-Atom Nanozyme for Boosted Tumor Therapy, 32 (2022) 2200331.
[24] Y. Zhu, W. Wang, J. Cheng, Y. Qu, Y. Dai, M. Liu, J. Yu, C. Wang, H. Wang, S.J.A.C. Wang, Stimuli-responsive manganese single-atom nanozyme for tumor therapy via integrated cascade reactions, 133 (2021) 9566-9574.
[25] X. Liang, N. Fu, S. Yao, Z. Li, Y.J.J.o.t.A.C.S. Li, The progress and outlook of metal single-atom-site catalysis, 144 (2022) 18155-18174.
[26] Q. Liu, A. Zhang, R. Wang, Q. Zhang, D.J.N.-m.l. Cui, A review on metal-and metal oxide-based nanozymes: properties, mechanisms, and applications, 13 (2021) 1-53.
[27] L. Shen, D. Ye, H. Zhao, J.J.A.C. Zhang, Perspectives for single-atom nanozymes: advanced synthesis, functional mechanisms, and biomedical applications, 93 (2020) 1221-1231.
[28] W. Wu, L. Huang, X. Zhu, J. Chen, D. Chao, M. Li, S. Wu, S.J.C.S. Dong, Reversible inhibition of the oxidase-like activity of Fe single-atom nanozymes for drug detection, 13 (2022) 4566-4572.
[29] S. Ji, B. Jiang, H. Hao, Y. Chen, J. Dong, Y. Mao, Z. Zhang, R. Gao, W. Chen, R.J.N.C. Zhang, Matching the kinetics of natural enzymes with a single-atom iron nanozyme, 4 (2021) 407-417.
[30] S. Wang, Z. Wang, Z. Li, X. Zhang, H. Zhang, T. Zhang, X. Meng, F. Sheng, Y.J.S.A. Hou, Amelioration of systemic antitumor immune responses in cocktail therapy by immunomodulatory nanozymes, 8 (2022) eabn3883.
[31] C. Zhao, C. Xiong, X. Liu, M. Qiao, Z. Li, T. Yuan, J. Wang, Y. Qu, X. Wang, F.J.C.C. Zhou, Unraveling the single atomic active site under realistic simulated natural heme-containing enzymes, 55 (2019) 2285-2288.
[32] M. Chen, H. Zhou, X. Liu, T. Yuan, W. Wang, C. Zhao, Y. Zhao, F. Zhou, X. Wang, Z.J.S. Xue, Single iron site nanozyme for ultrasensitive glucose detection, 16 (2020) 2002343.
[33] C. Zhao, C. Xiong, X. Liu, M. Qiao, Z. Li, T. Yuan, J. Wang, Y. Qu, X. Wang, F.J.C.c. Zhou, Unraveling the

enzyme-like activity of heterogeneous single atom catalyst, 55 (2019) 2285-2288.
[34] Q. Chen, S. Li, Y. Liu, X. Zhang, Y. Tang, H. Chai, Y.J.S. Huang, A.B. Chemical, Size-controllable Fe-N/C single-atom nanozyme with exceptional oxidase-like activity for sensitive detection of alkaline phosphatase, 305 (2020) 127511.
[35] H. Teymourian, A. Barfidokht, J.J.C.S.R. Wang, Electrochemical glucose sensors in diabetes management: An updated review (2010–2020), 49 (2020) 7671-7709.
[36] X. Liu, D. Huang, C. Lai, L. Qin, G. Zeng, P. Xu, B. Li, H. Yi, M.J.S. Zhang, Peroxidase-like activity of smart nanomaterials and their advanced application in colorimetric glucose biosensors, 15 (2019) 1900133.
[37] M. Adeel, K. Asif, M.M. Rahman, S. Daniele, V. Canzonieri, F.J.A.F.M. Rizzolio, Glucose detection devices and methods based on metal–organic frameworks and related materials, 31 (2021) 2106023.
[38] K. Xu, R. Zhou, K. Takei, M.J.A.S. Hong, Toward flexible surface-enhanced Raman scattering (SERS) sensors for point-of-care diagnostics, 6 (2019) 1900925.
[39] X. Gan, H. Zhao, R. Schirhagl, X.J.M.A. Quan, Non enzymatic fluorometric determination of glucose by using quenchable gC 3 N 4 quantum dots, 186 (2019) 1-10.
[40] R.G. Mahmudunnabi, F.Z. Farhana, N. Kashaninejad, S.H. Firoz, Y.-B. Shim, M.J.J.A. Shiddiky, Nanozyme-based electrochemical biosensors for disease biomarker detection, 145 (2020) 4398-4420.
[41] W. Zhao, G. Zhang, Y. Du, S. Chen, Y. Fu, F. Xu, X. Xiao, W. Jiang, Q.J.J.o.M.C.B. Ji, Sensitive colorimetric glucose sensor by iron-based nanozymes with controllable Fe valence, 9 (2021) 4726-4734.
[42] A. Galant, R. Kaufman, J.J.F.c. Wilson, Glucose: Detection and analysis, 188 (2015) 149-160.
[43] X. Fioramonti, C. Chrétien, C. Leloup, L.J.F.i.p. Pénicaud, Recent advances in the cellular and molecular mechanisms of hypothalamic neuronal glucose detection, 8 (2017) 875.
[44] Z. Peng, X. Xie, Q. Tan, H. Kang, J. Cui, X. Zhang, W. Li, G.J.J.o.I.O.H.S. Feng, Blood glucose sensors and recent advances: A review, 15 (2022) 2230003.
[45] L. Alvarado-Ramírez, M. Rostro-Alanis, J. Rodríguez-Rodríguez, J.E. Sosa-Hernández, E.M. Melchor-Martínez, H.M. Iqbal, R.J.B. Parra-Saldívar, Enzyme (single and multiple) and nanozyme biosensors: recent developments and their novel applications in the water-food-health nexus, 11 (2021) 410.
[46] L. Gao, J. Zhuang, L. Nie, J. Zhang, Y. Zhang, N. Gu, T. Wang, J. Feng, D. Yang, S.J.N.n. Perrett, Intrinsic peroxidase-like activity of ferromagnetic nanoparticles, 2 (2007) 577-583.
[47] H. Wei, E.J.A.c. Wang, Fe3O4 magnetic nanoparticles as peroxidase mimetics and their applications in H2O2 and glucose detection, 80 (2008) 2250-2254.
[48] S.R. Ahmed, J. Cirone, A.J.A.A.N.M. Chen, Fluorescent Fe3O4 quantum dots for H2O2 detection, 2 (2019) 2076-2085.
[49] Y. Jv, B. Li, R.J.C.c. Cao, Positively-charged gold nanoparticles as peroxidiase mimic and their application in hydrogen peroxide and glucose detection, 46 (2010) 8017-8019.
[50] S. Mvango, P.J.M.S. Mashazi, E. C, Synthesis, characterization of copper oxide-gold nanoalloys and their peroxidase-like activity towards colorimetric detection of hydrogen peroxide and glucose, 96 (2019) 814-823.
[51] G.J.N.R. Zhang, Functional gold nanoparticles for sensing applications, 2 (2013) 269-288.
[52] Y. Ziai, C. Rinoldi, P. Nakielski, L. De Sio, F.J.C.O.i.B.E. Pierini, Smart plasmonic hydrogels based on gold and silver nanoparticles for biosensing application, (2022) 100413.
[53] Z. Zhu, L. Garcia-Gancedo, A.J. Flewitt, H. Xie, F. Moussy, W.I.J.S. Milne, A critical review of glucose biosensors based on carbon nanomaterials: carbon nanotubes and graphene, 12 (2012) 5996-6022.
[54] Z. Wang, R. Zhang, X. Yan, K.J.M.T. Fan, Structure and activity of nanozymes: Inspirations for de novo design of nanozymes, 41 (2020) 81-119.

[55] W. Villena Gonzales, A.T. Mobashsher, A.J.S. Abbosh, The progress of glucose monitoring—A review of invasive to minimally and non-invasive techniques, devices and sensors, 19 (2019) 800.
[56] L. Jiao, W. Xu, H. Yan, Y. Wu, C. Liu, D. Du, Y. Lin, C.J.A.C. Zhu, Fe–N–C single-atom nanozymes for the intracellular hydrogen peroxide detection, 91 (2019) 11994-11999.
[57] N. Cheng, J.C. Li, D. Liu, Y. Lin, D.J.S. Du, Single - atom nanozyme based on nanoengineered Fe–N–C catalyst with superior peroxidase - like activity for ultrasensitive bioassays, 15 (2019) 1901485.
[58] L. Shen, M.A. Khan, X. Wu, J. Cai, T. Lu, T. Ning, Z. Liu, W. Lu, D. Ye, H.J.B. Zhao, Bioelectronics, Fe–N–C single-atom nanozymes based sensor array for dual signal selective determination of antioxidants, 205 (2022) 114097.
[59] Y. Feng, J. Qin, Y. Zhou, Q. Yue, J.J.J.o.C. Wei, I. Science, Spherical mesoporous Fe-NC single-atom nanozyme for photothermal and catalytic synergistic antibacterial therapy, 606 (2022) 826-836.
[60] N. Feng, Q. Li, Q. Bai, S. Xu, J. Shi, B. Liu, J.J.J.o.C. Guo, I. Science, Development of an Au-anchored Fe Single-atom nanozyme for biocatalysis and enhanced tumor photothermal therapy, 618 (2022) 68-77.
[61] X. Niu, Q. Shi, W. Zhu, D. Liu, H. Tian, S. Fu, N. Cheng, S. Li, J.N. Smith, D.J.B. Du, Bioelectronics, Unprecedented peroxidase-mimicking activity of single-atom nanozyme with atomically dispersed Fe–Nx moieties hosted by MOF derived porous carbon, 142 (2019) 111495.
[62] Y. Mao, S. Gao, L. Yao, L. Wang, H. Qu, Y. Wu, Y. Chen, L.J.J.o.H.M. Zheng, Single-atom nanozyme enabled fast and highly sensitive colorimetric detection of Cr (VI), 408 (2021) 124898.
[63] J. Ge, L. Yang, Z. Li, Y. Wan, D. Mao, R. Deng, Q. Zhou, Y. Yang, W.J.J.o.H.M. Tan, A colorimetric smartphone-based platform for pesticides detection using Fe-N/C single-atom nanozyme as oxidase mimetics, 436 (2022) 129199.
[64] R. Niu, Y. Liu, Y. Wang, H.J.C.C. Zhang, An Fe-based single-atom nanozyme with multi-enzyme activity for parallel catalytic therapy via a cascade reaction, 58 (2022) 7924-7927.
[65] C. Du, Y. Gao, H. Chen, P. Li, S. Zhu, J. Wang, Q. He, W.J.J.o.M.C.A. Chen, A Cu and Fe dual-atom nanozyme mimicking cytochrome c oxidase to boost the oxygen reduction reaction, 8 (2020) 16994-17001.
[66] C. Ma, S.-y. Xiao, Z.-g. Li, W. Wang, L.-j.J.J.o.c.A. Du, Characterization of active phenolic components in the ethanolic extract of Ananas comosus L. leaves using high-performance liquid chromatography with diode array detection and tandem mass spectrometry, 1165 (2007) 39-44.
[67] Y. Choi, S. Bae, B.-S. Kim, J.J.J.o.M.C.A. Ryu, Atomically-dispersed cobalt ions on polyphenol-derived nanocarbon layers to improve charge separation, hole storage, and catalytic activity of water-oxidation photoanodes, 9 (2021) 13874-13882.
[68] T. Nagata, Y.J.A.o. Obora, N, N-dimethylformamide-protected single-sized metal nanoparticles and their use as catalysts for organic transformations, 5 (2019) 98-103.
[69] L. Zhao, Y. Zhang, L.-B. Huang, X.-Z. Liu, Q.-H. Zhang, C. He, Z.-Y. Wu, L.-J. Zhang, J. Wu, W.J.N.c. Yang, Cascade anchoring strategy for general mass production of high-loading single-atomic metal-nitrogen catalysts, 10 (2019) 1278.
[70] G.V. Lowry, R.J. Hill, S. Harper, A.F. Rawle, C.O. Hendren, F. Klaessig, U. Nobbmann, P. Sayre, J.J.E.S.N. Rumble, Guidance to improve the scientific value of zeta-potential measurements in nanoEHS, 3 (2016) 953-965.
[71] J. Peng, W. Gao, B.K. Gupta, Z. Liu, R. Romero-Aburto, L. Ge, L. Song, L.B. Alemany, X. Zhan, G.J.N.l. Gao, Graphene quantum dots derived from carbon fibers, 12 (2012) 844-849.
[72] E. Dervishi, Z. Ji, H. Htoon, M. Sykora, S.K.J.N. Doorn, Raman spectroscopy of bottom-up synthesized graphene quantum dots: size and structure dependence, 11 (2019) 16571-16581.
[73] J. Wei, D. Xia, Y. Wei, X. Zhu, J. Li, L.J.A.C. Gan, Probing the oxygen reduction reaction intermediates and

dynamic active site structures of molecular and pyrolyzed Fe–N–C electrocatalysts by in situ Raman spectroscopy, 12 (2022) 7811-7820.
[74] R. Riaz, M. Ali, H. Anwer, M.J. Ko, S.H.J.J.o.c. Jeong, i. science, Highly porous self-assembly of nitrogen-doped graphene quantum dots over reduced graphene sheets for photo-electrocatalytic electrode, 557 (2019) 174-184.
[75] H. Namduri, S.J.C.S. Nasrazadani, Quantitative analysis of iron oxides using Fourier transform infrared spectrophotometry, 50 (2008) 2493-2497.
[76] L. Lin, Q. Zhu, A.-W.J.J.o.t.A.C.S. Xu, Noble-metal-free Fe–N/C catalyst for highly efficient oxygen reduction reaction under both alkaline and acidic conditions, 136 (2014) 11027-11033.
[77] P. Muhammad, S. Hanif, J. Li, A. Guller, F.U. Rehman, M. Ismail, D. Zhang, X. Yan, K. Fan, B.J.N.T. Shi, Carbon dots supported single Fe atom nanozyme for drug-resistant glioblastoma therapy by activating autophagy-lysosome pathway, 45 (2022) 101530.
[78] B. Jiang, D. Duan, L. Gao, M. Zhou, K. Fan, Y. Tang, J. Xi, Y. Bi, Z. Tong, G.F.J.N.p. Gao, Standardized assays for determining the catalytic activity and kinetics of peroxidase-like nanozymes, 13 (2018) 1506-1520.
[79] H. Dong, W. Du, J. Dong, R. Che, F. Kong, W. Cheng, M. Ma, N. Gu, Y.J.N.C. Zhang, Depletable peroxidase-like activity of Fe3O4 nanozymes accompanied with separate migration of electrons and iron ions, 13 (2022) 5365.
[80] X. Wang, T. Xiong, M. Cui, X. Guan, J. Yuan, Z. Wang, R. Li, H. Zhang, S. Duan, F.J.A.M.T. Wei, Targeted self-activating Au-Fe3O4 composite nanocatalyst for enhanced precise hepatocellular carcinoma therapy via dual nanozyme-catalyzed cascade reactions, 21 (2020) 100827.
[81] X. Zhang, C. Sun, R. Li, X. Jin, Y. Wu, F.J.A.C. Fu, Dual-Loading of Fe3O4 and Pd Nanoparticles on g-C3N4 Nanosheets Toward a Magnetic Nanoplatform with Enhanced Peroxidase-like Activity for Loading Various Enzymes for Visual Detection of Small Molecules, (2023).
[82] X. Zhou, M. Wang, J. Chen, X. Xie, X.J.A.C.A. Su, Peroxidase-like activity of Fe–N–C single-atom nanozyme based colorimetric detection of galactose, 1128 (2020) 72-79.
[83] Y. Gao, Y. Wu, J.J.S.A.P.A.M. Di, B. Spectroscopy, Colorimetric detection of glucose based on gold nanoparticles coupled with silver nanoparticles, 173 (2017) 207-212.
[84] H. Zhang, X. Liang, L. Han, F.J.S. Li, "Non-Naked" gold with glucose oxidase-like activity: a nanozyme for tandem catalysis, 14 (2018) 1803256.
[85] S.N. Prasad, S.R. Anderson, M.V. Joglekar, A.A. Hardikar, V. Bansal, R.J.B. Ramanathan, Bioelectronics, Bimetallic nanozyme mediated urine glucose monitoring through discriminant analysis of colorimetric signal, 212 (2022) 114386.
[86] D. Song, Y. Yang, T. Zhou, Y. Liu, S. Song, J. Zhang, H. Lu, Z.J.C. Zhao, Hybrid hydrogels based on insitu interpenetrating networks graphene oxide (GO) and Au nanoparticles, and its application as peroxidase mimetics for glucose detection, 3 (2018) 10259-10264.
[87] J.S. Park, J.S.J.S. Choi, A.B. Chemical, Platinum nanozyme-hydrogel composite (PtNZHG)-impregnated cascade sensing system for one-step glucose detection in serum, urine, and saliva, 359 (2022) 131585.
[88] W. Xu, L. Jiao, H. Yan, Y. Wu, L. Chen, W. Gu, D. Du, Y. Lin, C.J.A.a.m. Zhu, interfaces, Glucose oxidase-integrated metal–organic framework hybrids as biomimetic cascade nanozymes for ultrasensitive glucose biosensing, 11 (2019) 22096-22101.
[89] N.S. Vallabani, A.S. Karakoti, S.J.C. Singh, S.B. Biointerfaces, ATP-mediated intrinsic peroxidase-like activity of Fe3O4-based nanozyme: one step detection of blood glucose at physiological pH, 153 (2017) 52-60.
[90] H. Yan, L. Jiao, H. Wang, Y. Zhu, Y. Chen, L. Shuai, M. Gu, M. Qiu, W. Gu, C.J.S. Zhu, A.B. Chemical, Single-

atom Bi-anchored Au hydrogels with specifically boosted peroxidase-like activity for cascade catalysis and sensing, 343 (2021) 130108.
[91] N. Bagheri, M. Dastborhan, A. Khataee, J. Hassanzadeh, M.J.S.A.P.A.M. Kobya, B. Spectroscopy, Synthesis of g-C3N4@ CuMOFs nanocomposite with superior peroxidase mimetic activity for the fluorometric measurement of glucose, 213 (2019) 28-36.
[92] V.K. Gupta, N. Atar, M.L. Yola, M. Eryılmaz, H. Torul, U. Tamer, İ.H. Boyacı, Z.J.J.o.c. Üstündağ, i. science, A novel glucose biosensor platform based on Ag@ AuNPs modified graphene oxide nanocomposite and SERS application, 406 (2013) 231-237.
[93] K.V. Kong, Z. Lam, W.K.O. Lau, W.K. Leong, M.J.J.o.t.A.C.S. Olivo, A transition metal carbonyl probe for use in a highly specific and sensitive SERS-based assay for glucose, 135 (2013) 18028-18031.
[94] X. Bi, X. Du, J. Jiang, X.J.A.c. Huang, Facile and sensitive glucose sandwich assay using in situ-generated Raman reporters, 87 (2015) 2016-2021.
[95] Z. Han, X. Zhang, H. Yuan, Z. Li, G. Li, H. Zhang, Y.J.J.o.P.S. Tan, Graphene oxide/gold nanoparticle/graphite fiber microelectrodes for directing electron transfer of glucose oxidase and glucose detection, 521 (2022) 230956.
[96] G.E. Fenoy, W.A. Marmisollé, W. Knoll, O.J.S. Azzaroni, Diagnostics, Highly sensitive urine glucose detection with graphene field-effect transistors functionalized with electropolymerized nanofilms, 1 (2022) 139-148.
[97] P. Preechakasedkit, N. Nawaukkaratharnant, K. Teekayupak, A. Lomae, N.J.J.o.S.A.M. Ruecha, Devices, Single-preparation rGO/Cu–Cu2O nanocomposite-modified electrode integrating NaOH immobilized polymer blend film for one-step nonenzymatic glucose detection, 8 (2023) 100535.